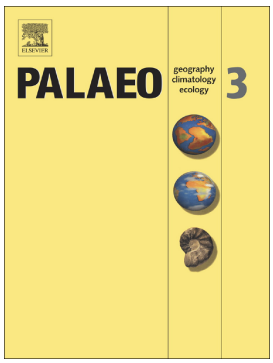

Ecosystem and landscape change in the 'Top End' of Australia during the past 35 kyr

K. Marx Samuel, William Reynolds, Jan-Hendrik May, Matthew S. Forbes, Nicola Stromsoe, Michael-Shawn Fletcher, Tim Cohen, Patrick Moss, Debashish Mazumder, Patricia Gadd

PII: S0031-0182(21)00444-2

DOI: https://doi.org/10.1016/j.palaeo.2021.110659

Reference: PALAEO 110659

To appear in: *Palaeogeography, Palaeoclimatology, Palaeoecology*

Received date: 2 April 2021

Revised date: 30 August 2021

Accepted date: 13 September 2021

Please cite this article as: K.M. Samuel, W. Reynolds, J.-H. May, et al., Ecosystem and landscape change in the 'Top End' of Australia during the past 35 kyr, *Palaeogeography, Palaeoclimatology, Palaeoecology* (2021), https://doi.org/10.1016/j.palaeo.2021.110659

Ecosystem and landscape change in the 'Top End' of Australia during the past 35 kyr

Samuel, K., Marx[1,*] smarx@uow.edu.au, William Reynolds[1,2] wgr299@uowmail.edu.au, Jan-Hendrik May[3,1] janhendrikmay@unimelb.edu.au, Matthew S., Forbes[2,7] matthewsforbes71@gmail.com, Nicola Stromsoe[4] nicola.stromsoe@cdu.edu.au, Michael-Shawn Fletcher[3] michael.fletcher@unimelb.edu.au, Tim Cohen[1,2] tcohen@uow.edu.au, Patrick Moss[5] patrick.moss@uq.edu.au, Debashish Mazumder[6,2] debashish.mazumder@ansto.gov.au, Patricia Gadd[6] patricia.gadd@ansto.gov.au

[1]GeoQuEST Research Centre - School of Earth, Atmospheric and Life Sciences, University of Wollongong, New South Wales, Australia.
[2]ARC Centre of Excellence for Australian Biodiversity and Heritage, University of Wollongong, New South Wales, Australia,
[3]School of Geography, University of Melbourne, Victoria, Australia
[4]College of Engineering, IT and Environment, Charles Darwin University, Northern Territory, Australia.
[5]School of Earth and Environmental Sciences, The University of Queensland, Queensland, Australia.
[6]Australian Nuclear Science and Technology Organisation, New South Wales, Australia.
[7]School of Biological Earth and Environmental Sciences, University of New South Wales, Australia.

[*]Corresponding author.

Abstract

The Indo-Australian Summer Monsoon (IASM) is the dominant climate feature of northern Australia, affecting rainfall/runoff patterns over a large portion of the continent and exerting a major control on the ecosystems of the Australia's Top End, including the viability of wetland ecosystems and the structure of the woody savanna, which characterises Northern Australia. We examined the behaviour the IASM from 35 ka using proxy data preserved in the sediments of Table Top Swamp, a small seasonal swamp in northern Australia. Elemental data, stable C and N isotopes, pollen and sedimentary data were combined to develop a picture of monsoon activity and ecosystem response. Results demonstrated that between 35-25 ka conditions were drier and more stable than present, with a more grass dominated savanna and limited wetland development, implying reduced IASM activity. After ~25 ka, there is evidence of increased moisture at the study site, but also increased IASM variability. However, despite evidence of at least periodic increases in moisture, including periods of wetland establishment, the IASM displayed a subdued response to peak precession insolation forcing by comparison to the other global monsoon systems. Instead, the greatest change occurred from ~10 ka when the continental shelf flooded, increasing moisture advection to the study site and resulting in establishment of a quasi-permeant wetland. Whereas the early Holocene was marked by both the onset of pollen preservation and a wetter vegetation mosaic, indicative of a consistently active IASM, the mid-late Holocene was marked by drier vegetation, increased fire, but also increased C_3 vegetation and runoff, implying increased IASM variability. Holocene changes in ecosystem dynamics occur coincident with an

expansion in human population, which likely also influenced vegetation and landscape response at the study site.

Key words: stable isotopes, Itrax, northern Australia, pollen, fire.

1. Introduction

Forming part of the larger Asian-Australian Summer Monsoon System (AASMS) and linked to the global monsoon system, the Indo-Australian Summer Monsoon (IASM) is the dominant climate feature of the wet-dry tropics of northern Australia (McRobie et al., 2015; Trenberth et al., 2000). It strongly influences water availability across Northern Australia, but also well south of the core monsoon region (Kajikawa et al., 2010; Kuhnt et al., 2015; Nicholls et al., 1982), such as within the southern Lake Eyre Basin in central Australia (Knighton and Nanson, 2001; Magee et al., 2004).

In particular, the IASM exerts a strong north-south rainfall gradient across Australia's 'Top End', the northern part of the Northern Territory, colloquially defined as north of 15°S, where mean annual precipitation (MAP) declines with distance from the axis of the monsoon trough and from the coast (Cook and Heerdegen, 2001). The strength of the IASM varies intra-seasonally to inter-annually (Kajikawa et al., 2010), with >90% of rainfall occurring during wet season months (between late October and late March) (Nicholls et al., 1982), and also over millennial time-scales (Denniston et al., 2013a; Denniston et al., 2013b; Eroglu et al., 2016; Ishiwa et al., 2019; Kuhnt et al., 2015).

The IASM is arguably the major control on the hydrology of the Top End (Pope et al., 2009), including for its numerous and diverse freshwater wetlands. These are typically seasonally ephemeral, with streamflow (runoff) displaying high seasonality and inter-annual variability, even by comparison to similar climates elsewhere (Petheram et al., 2008), and annual evaporation exceeding MAP (i.e., 2.53 versus 1.72 m/yr at Darwin). Wetland dynamics are therefore highly coupled to changes in IAMS activity (Bird et al., 2019), with sediments preserved in these wetlands expected to contain valuable records of past IASM activity (Rowe et al., 2019; Rowe et al., 2020).

Existing studies imply that the IASM has been highly dynamic through time, exhibiting a spatially variable response over the last glacial cycle (McRobie et al., 2015). For example, the IASM may have responded differently to events such as Heinrich Event 1, the Bølling–

Allerød and Younger Dryas across the Indo-Australian region (Ayliffe et al., 2013; Mohtadi et al., 2011; Partin et al., 2007; Yan et al., 2015). This highlights the need for records of IASM records from throughout its zone of influence. The IASM also potentially exhibits a more complex response to forcing factors than the Northern Hemisphere monsoon systems (Liu et al., 2003; Marshall and Lynch, 2008; McRobie et al., 2015). Whereas millennial-scale variability in the African, South American and other parts of the Asian monsoon have been strongly linked to Northern Hemisphere precession-driven insolation variability (Cruz et al., 2005; Gasse, 2000; Rossignol-Strick, 1985; Ruddiman, 2006; Yuan et al., 2004), the IASM has displayed a more subdued response, possibly because the IASM is influenced by a number of additional drivers. For example, over the past glacial cycle changes in IASM activity have been linked to (Northern and Southern Hemisphere) precession-driven insolation change (the orbital monsoon hypothesis) (Liu et al., 2003; Magee et al., 2004; Marshall and Lynch, 2008; Mohtadi et al., 2011; Ruddiman, 2006; Wyrwoll and Valdes, 2003), sea surface temperature (SST) (Liu et al., 2003; Marshall and Lynch, 2008), sea level (Marshall and Lynch, 2008) and abrupt Northern Hemisphere climate change (e.g., Heinrich events) (Ayliffe et al., 2013; Denniston et al., 2017; Mohtadi et al., 2011; Partin et al., 2007). Additionally, IASM activity has also been attributed to changing atmospheric composition (Ayliffe et al., 2013) and even human induced vegetation change (Miller et al., 2005). This again highlights the need for records of past IASM activity from different locations where these factors may be more or less significant.

In Northern Australia, the IASM has a significant influence on ecosystem processes, composition and dynamics (Bowman et al., 2010a), as well as potentially also influencing ecosystems across central Australia (Johnson et al., 1999). This includes influencing the composition and occurrence of savannas, the dominant vegetation community of Northern Australia, which are thought to be strongly influenced by high seasonality in moisture availability and the prolonged (7 month) dry-season (Cook and Heerdegen, 2001; Sankaran et al., 2005; Staver et al., 2011a). For example, the abundance of tree versus grass cover in savannas changes in space, with tree cover, height, basal area and woody species richness decreasing away from the coast along the rainfall gradient (Williams et al., 1996). In the context of this study, it is important to note, that the factors influencing tree-grass dynamics in the Australian savannas are not fully understood and include parameters not directly related to climate. This includes the role of burning by humans, herbivory and nutrient availability (Beringer et al., 2015; Bowman et al., 2010b; Fensham et al., 2003; Hill and Hanan, 2010), as well as global scale changes in atmospheric CO_2 ($[CO_2]_{atm}$), which

influences C_3 grass abundance (Gerhart and Ward, 2010). In addition, it has been proposed that the current tree/grass composition is a result of palaeo-disturbance (fire, drought, herbivory and nutrient availability), rather than present conditions (Fensham et al., 2009; Sankaran et al., 2005; Staver et al., 2011b). Despite this, temporal variability in water availability is considered to directly influence the relative productivity of trees and grasses (Moore et al., 2018; Prior et al., 2004; Prior et al., 2009).

The wetlands of Northern Australia occur intermittently amongst the surrounding savanna. They are highly productive ecosystems which support many important flora and fauna (Warfe et al., 2011) and are culturally important for Australia's indigenous people (Jackson et al., 2005). Similar, to savanna, their ecological composition is hihgly linked water availability and IASM activity (Bird et al., 2019).

Although variability in the IASM strength is anticipated to have resulted in significant changes to the terrestrial and freshwater systems of Northern Australia over millennial timescales (Yan et al., 2015), few studies have examined palaeo-behaviour of the IASM within its core region, north of the monsoon trough (e.g. Denniston et al., 2013b; Kuhnt et al., 2015; Mohtadi et al., 2011). Similarly, despite its role in ecosystem dynamics, very few Australian have examined ecosystem change in response to IASM variability (Field et al., 2018c; McGowan et al., 2012; Stevenson et al., 2015; van der Kaars et al., 2006), especially in the Top End (Rowe et al., 2019; Rowe et al., 2020). This is despite high potential for preservation of palaeo-environmental information in the numerous wetlands across the Top End and recent advances in establishing more reliable chronologies in these challenging sedimentary environments (Field et al., 2018b; May et al., 2018). The aim of this paper is to reconstruct past variability in ecosystem structure and water availability in a seasonal swamp within the monsoon (wet dry) tropical savanna of the Top End, and to use changes in these parameters to examine the operation of the IASM over that period.

2. Regional Setting

Table Top Swamp (TTS) (13.178° S and 130.746 °E, 200 m AHD) is a seasonally ephemeral swamp located on the top of the Table Top Range, a sandstone Plateau ~200 m above sea level and ~75 km inland (Fig. 1a). It is within the zone of *direct* monsoon influence, defined by the presence of strong cross-equatorial flow, seasonal wind direction reversal and strongly seasonal rainfall, which encompasses the region of the Australian

continent, north of ~15°S and between 120°E and 150°E (Kajikawa et al., 2010; Kuhnt et al., 2015).

The swamp occupies a small depression within a catchment of approximately 0.75 km^2. Its small catchment and very limited groundwater contribution (see Supplementary Information) make TTS an excellent environment to reconstruct changes in IASM activity, which are manifest most readily as changes in precipitation. These are expected to be are preserved in the swamp sediments via changes to sediment delivery/composition, swamp hydrological status and biological composition/production.

The TTS catchment sits within the 1840 Ma Paleoproterozoic Depot Creek Sandstone consisting of medium to very coarse clean quarzitic sandstone with minor quartz pebble conglomerate beds (Ahmad and Hollis, 2013; Ahmad et al., 1993; Hollis and Glass, 2011). Extensive Fe-cemented ferruginous rubble laterites outcrop in the catchment (Pietsch, 1989; Pietsch and Edgoose, 1988). Soils are shallow and well drained.

Vegetation on the plateau is dominated by *Eucalyptus* savanna (open forest and woodland with a grassy or shrub/grass understorey), typical of the Top End, with monsoon rainforest or gallery forest located in areas offering more permanent access to water or protection from fire (Kirkpatrick et al., 1987) (Fig. 1e). In the savanna woodland surrounding TTS the dominant overstorey species include *Eucalyptus tetradonta* (Darwin stringybark) and *E miniata* (Darwin woolybutt), while understorey species include the grasses *Triodia microstachya* (spinifex), *Germania grandiflora*, *Eriachne shultzeana, E. triseta, Heteropogon triticeus* and *Sorghum intrans* and shrubs *Hibbertia spp., Planchonia careya and Acacia spp*.. The littoral zone, an approximately 30 m band around the swamp, is dominated by *Melaleuca viriflora* woodland, while mesic emergent vegetation (incl. *Typha spp.* and *Cyperaceae*), grow on the swamp surface (Fig. 1c).

Rainfall is highly seasonal with >90% of precipitation occurring in the summer half of the year (between November and April) . MAP at Table Top Swamp is 1900 mm, (Bureau of Meteorology (BOM) gauges #014272 and #014272). Mean monthly maximum temperatures are 34°C in both wet and dry seasons, while mean monthly minimum temperatures are 24°C and 20°C in the wet and dry season, respectively. Potential evaporation is 2,200 mm/year (Montanari et al., 2006), resulting in a dry season water deficit. Consequently, the moisture status of TTS is highly seasonal with swamp water levels ranging between 2.6 m during the wet season (above which it spills into Wangi Creek) and 0 m depth at the end of the dry season (Fig. 1c and d).

Prior to the 1940s, most of the Top End including the area around TTS was managed traditionally by Aboriginal people, who used burning to actively manage the landscape and resources for thousands of years (Preece, 2013). Changes in fire regimes, including the introduction and then disruption of Aboriginal land management, have likely played a role in vegetation (tree-grass) dynamics in the northern savannas. For example, anthropogenic burning may have reduced the strength of the IASM in Australia during the Holocene (Miller et al., 2005), although this is disputed (Pitman and Hesse, 2007).

3 Methods

3.1 Sample collection and processing

A 1.18 m (TS-425) core was extracted from the centre of the TTS using a vacuum-sealed aluminium tube, which was manually hammered into lakebed. At the University of Wollongong, the core was split lengthwise. One half was scanned using an Itrax core scanner (described in section 3.2) then sliced into segments (samples) of 2 mm length for the upper 400 mm, then 5 mm for the remainder of the core. A suite of analyses were undertaken these samples, including grainsize, while pollen, charcoal, stable isotope ($\delta^{13}C$ and $\delta^{15}N$) and elemental analysis (Total Organic C (TOC) and N) were undertaken on selected samples. Samples of catchment vegetation and soils were collected to characterise the $\delta^{13}C$ of potential sources of OM to the TTS record. This included sampling sedges, modern peat and algae from within the swamp itself. The remaining half of the core was sampled for geochronology.

3.2 Itrax core scanning

Semi-quantitative characterisation of the elemental chemistry of the core was obtained using an Itrax micro energy dispersive X-ray fluorescence radiation core scanner (μXRF). Full description of the Itrax score scanner is given by Croudace and Rothwell (2015). Elemental counts were obtained for 38 elements: Al, Si, P, Cl, K, Ca, Sc, Ti, V, Cr, Mn, Fe, Co, Ni, Cu, Zn, Ga, Br, Rb, Sr, Y, Zr, Pd, Ba, Hf, Ta, Tm, Er, Ho, Dy, Eu, Sm, Nd, Ce, La, W and Pb, using a Mo x-ray source at 30kV and 55 mA with step time of 2 mm and an exposure time of 20 s.

3.4 Sedimentary analysis

Grain size for each core sample (n=357) was analysed by laser diffraction using a Malvern Mastersizer 2000. Prior to analysis organics were removed by loss on ignition at

450°C and samples were dispersed using 10 s of ultrasonication. Visual and tactile inspection prior to analysis indicated sample textures were within the capacity of the Malvern Mastersizer, therefore samples were not sieved prior to analysis. Grain size distributions for each sample were calculated as the average of five analyses undertaken with 20 s of measurement time.

The carbonate content of samples in the core was examined by both HCl digestion and by loss on ignition following the procedure outlined in Heiri et al. (2001).

3.5 Pollen and charcoal analysis

Twenty-five sub-samples were selected for pollen and charcoal analysis. Pollen/charcoal was isolated following van der Kaars (1991), and Moss (2013). Samples were disaggregated using 10 % $Na_4P_2O_7$ at 100 ºC. Exotic *Lycopodium* spores, of a known concentration, were added to each sample. Samples were sieved between 8 - 180 µm. Humic acids were removed with 8 % KOH at 90 ºC, after which $Na_6O_{39}W_{12} \pm H_2O$ (specific gravity 2.1) was used to isolate organics from mineral matter. Samples then underwent acetolysis (using a 9:1 ratio of CH_3CO_2H and H_2SO_4). For identification, samples were mounted on glass slides, using glycerol, and counted using transmitted light microscopy at ×400 magnification. Counting of *Lycopodium* spores enabled calculation of pollen and charcoal concentrations. Three hundred grains of dryland pollen were counted in each sample. Charcoal was counted by undertaking three transects across each slide, with all black angular fragments >5 µm counted as charcoal.

3.6 Stable isotope analyses

Total organic carbon (TOC), total organic nitrogen (TON), stable nitrogen ($\delta^{15}N_{TON}$) and carbon ($\delta^{13}C_{TOC}$) isotopes were measured on 23 samples through the core. Prior to analysis samples were oven-dried at 45 °C for 72 hours then acidified with 0.1 M HCl for one hour and gently rinsed with Milli-Q water to remove remaining acid (Mazumder et al., 2010). Samples were re-dried and ground to a fine powder with a mortar and pestle before isotope analysis. Samples were analysed on a continuous flow stable isotope mass spectrometer (GV Instruments IsoPrime EA/IRMS) at ANSTO. Multiple analyses of standards, including samples analysed alongside TTS samples are reported in Table S1. Stable isotope values were reported in delta (δ) units in parts per thousand (‰) relative to the international standard Vienna Pee Dee Belemnite limestone ($^{13}C/^{12}C$ = 0.0112372) for

$\delta^{13}C$ and nitrogen in the air (0.03676) for $\delta^{15}N$ and determined as follows: $(R_{sample}/R_{standard} - 1)x1000$, where R is the $^{13}C/^{12}C$ or $^{15}N/^{14}N$ ratio, respectively.

3.7 Geochronology

Geochronology for TS-425 involved the application of optically stimulated luminescence (OSL) and radiocarbon dating, as outlined in May et al. (2018). Spatially highly-resolved measurements of the bulk OSL signal (Ln and Ln/Tn) were undertaken to help constrain the age-depth structure of the core. When normalised against dose rate, these provide information on the stratigraphic integrity of the core allowing identification of changes to the sedimentation rate, hiatuses or unconformities.

3.8 Modelling palaeo-hydrological conditions in TTS

A space for time substitution was used to model the effects of changing coastline proximity on TTS hydrology. Present day precipitation in the Top End is influenced by continentality (Fig.1). For example, MAP on the coast at Darwin (13.5°S) is 1,700 mm/yr, compared to 970 mm/yr at Katherine and 450 mm/yr at Tennant Creek, 240 and 850 km inland, respectively (equating ~-1.5-3 mm/km). This rainfall gradient implies the changing coastline position during the Quaternary would have influenced moisture advection to TTS.

This effect of changing coastline position through time was examined using the present day rainfall gradient to infer past hydrological conditions at TTS for different coastline positions. Coastline position within Joseph Bonaparte Gulf was previously reconstructed at specific time steps (18, 12, 9 and 6.5 ka) using numerical models and sediment cores by Yokoyama et al., (2001). At 18 ka (and through the LGM), the entire continental shelf was exposed, with the coastline located ~530 km north of its present position. By 12 ka rising sea level resulted in approximately half the continental shelf being flooded, with the coastline ~200 km from its current position. After 9 ka the continental shelf was extensively flooded with the coastline close to its current position (Yokoyama et al., 2001). Precipitation at 18 and 12 ka at TTS was estimated using the rainfall records from climate stations located at the equivalent distance from the modern coastline (~500 and ~200 km inland) (see S1). Swamp hydrodynamics at these time steps were then estimated using a water balance equation:

$$V_t = ((P - E1) \times As) + (((P-Etc) \times Ac)*Rc) \quad (1)$$

Where V_t = swamp water volume at time t, P = precipitation, $E1$ = swamp (pan) evaporation, Etc = catchment evapotranspiration, A_s = swamp area, Ac = catchment area and Rc = the runoff coefficient. Swamp capacity (water holding volume) was adjusted at the 12 and 18 ka time-steps based on the sedimentation in the TTS core. Model parametrisation, sensitivity and accuracy are outlined in S1.

It is important to note other factors, most significantly sea surface temperature (SST), also influence rainfall over northern Australia at sub-annual, multi-annual (Jourdain et al., 2013; Nicholls, 1995) and likely millennial time-scales (Marshall and Lynch, 2008), but are not taken into account by this approach. In addition, evaporation/evapotranspiration would differ through time in response to changes in temperature, wind-speed and cloudiness. Constraining these changes through time is complex. For example, reduced temperatures at 12 and 18 ka would reduce evaporation/evapotranspiration at TTS, however, reduced humidity resulting from a more distant coastline would increase evaporation. As the purpose of modelling swamp hydrodynamics was to investigate the effect of the changing positon of the coastline alone, modern evaporation/evapotranspiration values were using in Equation 1 at both the 12 and 18 ka time-steps. Use of modern values limits the usefulness of the hydrological model, however, the effect changes in in evaporation/evapotranspiration on swamp hydrology at TTS are estimated to be <10% at both the examined time-steps (see S1).

4. Results

4.1 Sedimentary characteristics of TTS

Based on colour, texture and organic matter six sedimentary units were identified in the TTS core (Fig. 2a-d).

Unit 6 (1181-1100 mm); consisted of yellowish red (5YR 4/6) to brown (7.5YR 5/2) sandy clay. Clay reached its highest (~40%) and silt its lowest (generally <20%) proportions within the core, while TOC was less than ~1%.

*Unit 5 (1100-790 mm);*exhibited consisted of a transition from a brown (7.5YR 5/2) sand/loamy sand below 950 mm to a dark grey (5YR 4/1) loam above this depth. Sand content was 80% at the base of the unit (the highest in the core) and 40-50 % at the top. Silt content increased from <30, to 40-50 % through the unit. A pronounced clay spike (40%) marked the Unit 5/4 transition. TOC remained below 1%.

Unit 4 (790-500 mm); comprised dark grey (5YR 4/1) silty loam. Silt increased from 65 to 75% in the unit, while clay and sand decreased from 15-20 to 10% and ~20 to 10%, respectively.

Unit 3 (500-400 mm); consisted of a silty loam and was marked by the presence of distinctive strong brown mottles (7.5YR 5/6) within a dark grey matrix (5YR4/1), indicative of significant Fe precipitation. Sand increased from <10 to >10%, while TOC remained low.

Unit 2 (400-190 mm); was comprised of silty loam. It was characterised by a colour transition to a very dark greenish grey (Gley 3/10Y), reflecting increasing TOC content from <1% to 5-7% through the unit.

Unit 1 (190-0 mm); was a dark bluish black organic rich sediment (Gley 2.5/5PB). It was characterised by high TOC,~20%. Below 100 mm the texture of Unit 1 consisted of silt, while above this depth sand content reached 40% and the texture approached that of a silty loam. Clay content was at its lowest proportion in Unit 1, typically <5%. Carbonate was present throughout the core at concentrations of 3-11% by weight.

4.2 Itrax µXRF

In situ elemental counts produced by µXRF core scanning are known to be influenced by changes in organic content (the closed-sum effect), the degree of decomposition, water content and density (Löwemark et al., 2011), in addition to elemental abundance and instrument precision. It is therefore necessary to examine the performance of individual elemental counts.

A Runs Test for randomness (Fu and Koutras, 1994) was performed on elemental counts. Results indicated P, S, Zn, Sn and Pr displayed statistically ($P<0.05$) random counts. Other elements (Al, Cl, Mn, Cu, Br, Zr, Ba, La, Pr, Nd, Sm, Eu, Dy, Ho, Er, Tm and Pb) returned low counts (>10% of the data = 0 cps) or displayed a high degree of noise (V, Ni, Rb, Sr, Pd, Ce and Ta) when plotted against depth, obscuring their interpretation in some cases. With the exception of Sr (which was less noisy), these elements were largely excluded from further discussion. Remaining elements (Si, K, Ca, Ti, Cr, Fe, Ga, and Y) displayed coherent count patterns and were used to interpret palaeo-processes at TTS.

To approximate conventional XRF concentrations, counts of remaining elements were converted to centred natural log ratios following Weltje and Tjallingii (2008). Transformed elemental counts generally displayed a significant reduction in the top 200 mm (Unit 1) of the core (returning negative values). This is shown by way of example for Ti in Figure. 2d. Below 200 mm depth (Units 2-6) counts varied. Titanium displayed relatively high counts in

Units 6 and 5 (~800 mm), before decreasing in the overlying units (Fig. 2d). This pattern was also evident for K (Fig. 2d), Cr, and Ga and for Sr and Rb, despite greater noise in their signals (not shown).

By contrast, Si and Ca displayed highest counts between Unit 4 and 2 (800-200 mm depth) (Fig. 2d). In contrast to most elements, Y counts increased within Units 1 and 2, with peak counts centred at ~200 mm depth. This pattern was also displayed by Zr, Nd, Sm and Tm (not shown), although these elements returned more significant numbers of zero counts (>10-18%). Lastly, Fe displayed a unique pattern, with two regions of higher values; at the base of the core below ~1000 mm depth and between the top of Unit 4 and bottom of Unit 2 (600-400 mm) (Fig. 2d).

4.3 Pollen and charcoal

A total of 35 taxa were identified at TTS (Fig. 3). These were divided into groups, based on life form; arboreal taxa, herbs, Pteridophyte and aquatic taxa. No pollen was observed below Unit 3 (>500 mm). Herbaceous taxa, chiefly Poaceae, and arboreal taxa (largely the Myrtaceous genera *Eucalyptus* and *Melaleuca*) dominate the record, comprising 60 and 35% of total pollen, respectively. The abundance of Aquatic taxa, including *Typha*, Cyperaceae, *Polygonum* and Nymphaceae varied, comprising 0-45% of total pollen. Pteridophyte taxa had negligible representation in the record. Charcoal was present in Units 5 to 1. Concentrations reduced between Units 5 and 4, with little charcoal present in Unit 3. Above 350 mm depth (Unit 2), charcoal increased toward the top of the core. In addition to pollen and charcoal, the core contained abundant diatoms and sponge spicules throughout.

Two main pollen groups are identifiable in TTS (Fig. 3), corresponding with Units 1 and 2. Lower pollen and charcoal concentrations occurred in Unit 2, which contained higher concentrations of moisture demanding, fire-sensitive genera, including Arecaceae, *Ficus*, *Callitris*, *Pandanus* and Casuarinaceae. It also contained relatively higher concentrations of aquatic taxa, chiefly, *Typha* and Cyperaceae. By comparison, Unit 1 contained more abundant Myrtaceous taxa. Poaceae abundance increased, reaching 50-65% of the total pollen sum in top of the core. The diversity of arboreal taxa also increased in Unit 1, with *Celtis*, *Terminalia*, *Bombax*, *Dodonaea*, Sapotaceae and Sapindacae present in small quantities.

One additional sample from Unit 3 contained pollen, although pollen was not preserved immediately above or below this sample. It contained a high abundance of *Ficus* and Arecaceae (Palm pollen) in particular, but contained a very low pollen concentration. It

presence may indicate TTS was a refuge at this time, although it also seems unlikely that *Ficus* would dominate woody vegetation anywhere in northern Australia and other northern Australia pollen records show no evidence of this (e.g., Field et al., 2017; Rowe et al., 2019; Rowe et al., 2020). Therefore, this could be the result of selective preservation.

4.4 Carbon and nitrogen

As previously outlined, Total Organic Carbon (TOC) content in the TTS core was approximately 0.1% in Unit 6, increasing to >1% above ~300 mm depth (Unit 2) and reaching 20% in the top 200 mm of the core (Fig. 2c). C/N ratios largely followed the TOC pattern with ratios ~5 in Units 6 to 2, increasing in Unit 2 to a peak of ~19 at the Unit 2/Unit 1 transition. In contrast to TOC, C/N ratios then decreased to ~16 in the remainder of Unit 1. $\delta^{13}C_{TOC}$ values ranged between -18 and -26.5‰ (Fig. 2c). It was most enriched in Units 6 and 5 (<-20 ‰) becoming more depleted in Unit 4-3. In Unit 2 and 1, $\delta^{13}C_{TOC}$ values became significantly more depleted with values of -24‰ to -26‰ above 250 mm. $\delta^{15}N$ values displayed a similar pattern to $\delta^{13}C_{TOC}$ values (r^2=0.95), with greatest enrichment in Units 6 and 5 (values of ~+5‰). Above Unit 5, $\delta^{15}N$ was more depleted, values decreased from ~+3.5 to +1‰ within Unit 2 and were <1‰ in Unit 1.

$\delta^{13}C$ values from modern vegetation and soil from TTS and TTS catchment were largely around -30‰ (Table 1). Leaves and bark of Proteaceae (*Grevillea* and *Banksia*), Myrtaceae (*Eucalyptus* and *Melaleuca*) and Cyperaceae species all fell in the range of -33 to -27‰. A Poaceae species was the only C_4 vegetation sample analysed, with a $\delta^{13}C$ value of -12.5‰. Leaf litter samples exhibited $\delta^{13}C$ values between -32 to -29‰.

4.5 Dating results and age model construction

OSL and radiocarbon ages and Ln/Tn DR_{norm} results were previously discussed in detail in May et al., (2018). Based on those results, an age model was constructed for the core from ^{14}C ages not deemed outliers and from OSL ages using the BACON model (Blaauw and Christen 2011) (Fig. 4). The modern surface was assigned an age of zero years. Using the Ln/Tn DR_{norm} ratios, either very slow sedimentation or hiatuses/unconformities were suspected at two intervals, between ca. 400 and 500 mm, and 700 and 800 mm depth (see May et al., 2018). These depths were used to define boundaries in the age model. The resulting age model is expressed as an age estimate at 1 mm intervals, with an uncertainty value averaged from upper and lower age boundaries around a median value.

The age model implied the base of the core dates from 38.6 ±7.4 ka. As there were no measured ages below Unit 5, the modelled age of 35.2 ±6.3 ka, at the stratigraphic boundary between Units 5 and 6 (~1106 mm depth), represents an alternative estimate for the onset of sedimentation in TTS (Fig. 4).

Four distinct chronological zones were evident from the TTS age-model. These were separated by distinct ages/age clusters (at >1sigma for OSL and > 2 sigma for radiocarbon), and/or are bounded by changes in the Ln/Tn DR_{norm} profile (Fig. 4). The base of Zone 1 (1106 and 750 mm depth), corresponds to late MIS3 to early MIS2 and Unit 5. It was constrained by an OSL age of 30.8 ±3.7 ka (1108 mm) which overlapped with the age at 950 mm (32 ±3.6 ka). The sedimentation rate in Zone 1 was ~0.025 mm/yr, while age uncertainty was ±19%, equating to >5 ka.

Zone 2 encompasses the LGM to Pleistocene/Holocene transition and Unit 4. The start of Zone 2 is demarked by a rapid drop in Ln/Tn DR_{norm} ratios and an OSL age of 25 ±2.4 ka. Its base is marked by a radiocarbon age of 8.1 ±0.5 ka. Zone 2 contains limited age control, due to its fine texture and absence of organics (Fig. 2b and c). The significant down-profile variability in Ln/Tn DR_{norm} ratios in Zone 2 their sharp contrast the ratios in Zone 1, imply depositional hiatuses and/or periods of very slow sedimentation. Zone 2 is characterised by high age uncertainty (±22%).

Zones 3 and 4 encompass the Pleistocene/Holocene transition to Mid-Holocene (Zone 3) and Mid-Holocene to present (Zone 4). These zones are constrained by ^{14}C ages of between 8.1 ±0.5 and 4.4 ±0.6 ka and 4.4 ±0.25 and 0 ka, respectively. They are are characterised by faster sedimentation rates (0.041 and 0.051 mm/yr), and lower age uncertainty (±5 and ±12 %, equating to 0.2 and 0.3 ka, respectively). The Ln/Tn DR_{norm} ratios through both zones displays a steady decrease, implying consistent and relatively fast sedimentation.

4.5 Past Hydrology of TTS.

The output from the hydrological model provides a broad snapshot of potential hydrological conditions at TTS. Results indicate that at the 18 ka time-step TTS remained dry for ~50% of the time (50% of days/year), filling to capacity/over-topping ~10% of the time (Fig. 5). By comparison, modelling (and observation) of modern conditions indicate TTS is dry ~20% of the time (at the end of the dry season) and filling/over-topping ~35% of the time. This implies TTS was ~30% drier during the LGM.

By 12 ka approximately ½ the continental shelf within Joseph Bonaparte Gulf was flooded (Yokoyama et al., 2001). TTS likely experienced hydrological conditions somewhat similar to today, although possibly drier. Results indicated that at this time TTS was dry ~30% of the time and full/over-topping ~30% of the time (i.e. a 5-10 % difference from modern conditions).

5. Discussion

In this discussion, we examine past-process/biological activity in TTS as inferred by Itrax μXRF. We then use a $\delta^{13}C$ endmember mixing-model to estimate changing vegetation composition and use $\delta^{15}N$ values to examine potential rainfall changes at TTS. These datasets are then used, alongside the other proxy datasets and the results of previous studies to infer the past behaviour of the IASM and examine ecosystem response at TTS.

5.1 Palaeo-processes at TTS inferred from geochemical data

Changes to elemental abundance, revealed by μXRF core scanning, can be used to examine past physical and biological processes at TTS. High normalised Ti counts suggests TTS was dominated by the deposition of mineral material (Fig. 2d) between 35 to >25 ka (Zone 1). Between ~25 and 5 ka, Ti counts decreased, indicating other processes were more significant. In contrast to Ti, Ca and Si counts increased after ~25 ka. This most likely is caused by increased fixation of Ca in organic matter or in $CaCO_3$ shells and Si in the frustules of algae and spicules of sponge (well preserved spicules and diatoms were evident throughout the core, and carbonate was present throughout the core). Alternatively, changes in Si and Ca counts might be explained by increased (decreased) deposition of weathering products and/or in *in situ* mobility of these elements due to solution/precipitation processes in the swamp.

Changes in the delivery of weathering products or *in situ* mobility of Si and Ca (and other elements) can be examined by comparing down-core patterns in these elements to those of Sr and Fe, which are highly mobile/weathering affected (Kamber et al., 2005; Marx and Kamber, 2010; Nesbitt et al., 1980). Both the Si and Ca profiles in TTS contrast with Sr, the pattern in which resembles that of Ti, with highest counts before ~25 ka (Fig. 2d). Similarly, neither element matches Fe, which contains prominent peaks in counts at 500 and 1100 mm depth (marked by a distinct orange colouration and mottling). These Fe peaks are the result

from Fe oxyhydroxide precipitation in response to seasonal water-table variability (Fig. 2a). Therefore, changes in Si and Ca counts are largely the result of biological concentration.

After 5 ka counts for most elements became negative due to dilution of mineral material by organic matter. Counts of some elements increased, however. This included the conservative element Y, as well as Zr, Nd, Sm and Tm, (despite these having significant zero counts). This represents either a change in sediment provenance and/or delivery of more weathered sediment. Although typically regarded as conservative (Kamber et al., 2005; Marx and Kamber, 2010), these elements can be mobile during enhanced weathering, as would be expected in the high weathering environment (high rainfall and temperatures) of the Top End, and as occurs during laterite formation (Babechuk et al., 2015; Hill et al., 2000). Changes in counts of these elements therefore results from either an increased contribution from catchment laterite, changing aeolian dust input, or increased delivery of weathering products.

Palaeo-processes at TTS can be examined in more detail using element ratios which can more definitively elucidate environmental processes (e.g. Marx and Kamber, 2010). The ratio of Sr to Ca has been used as an indicator of relative evaporation in lake systems subject to drying, where precipitation of Sr from solution occurs more rapidly than Ca (Chen et al., 1999; Grosjean et al., 2001; Olsen et al., 2013). In the case of TTS, evaporation of water during the prolonged dry season leads to the concentration of carbonates. The Sr/Ca ratio is relatively high prior to ~25 ka, implying drier conditions at this time, i.e. increased evaporative precipitation of Sr (Fig. 6c).

Silicon/Ti has been used to approximate biological production by Si concentrating organisms (sponges, diatoms and plants (phytoliths)) (e.g., Brown, 2015; Brown et al., 2007; Field et al., 2018a; Kylander et al., 2011). In some environments, Si/Ti ratios are influenced by, and have been used to infer, grainsize. This occurs where Ti is concentrated in secondary clay minerals weathered from Ti minerals such as biotite. However, the catchment of TTS, within a Paleoproterozoic sandstone, contains little clay. Rather in quartz-rich sandstones, like the Depot Creek Sandstone, Ti is predominately hosted in weathering resistant minerals, including rutile and ilmenite, and as such as no link to grainsize (i.e., the R^2 between mean grainsize and Si/Ti in TTS is 0.07). The abrupt increase in Si/Ti ratios in TTS after ~25 ka is therefore likely the result of enhanced biogenic Si production in this context, from which increased moisture availability in the swamp can be inferred (Fig. 6c).

Calcium can also be indicative of biological production, both from organisms and plants concentrating Ca (Lauterbach et al., 2011; Olsen et al., 2013). Similar to Si, the ratio

of Ca to more conservative elements (such as Ti or Ta) increases after ~25 ka, again possibly due to enhanced biological productivity, again indicating increased moisture/enhanced IASM activity. Calcium/conservative element ratios (e.g. Ca/Ti) increased further in the top 2 ka of core, where living root material was more abundant, reflecting the concentration of Ca in organic matter (Fig. 6d). It should be noted, however, that changes in Ca can provide different palaeo-environmental information in different contexts (Davies et al., 2015), e.g., Ca is highly weathering sensitive (Nesbitt et al., 1980). Therefore, increased Ca/conservative element ratios after ~25 and ~5 ka could result from increased biological activity, or weathering, or both. Iirrespective of the cause, this indicates increasing moisture at TTS.

Increases in the ratio of weathering sensitive elements to conservative elements like Ti, (which is very highly resistant to weathering (Hill et al., 2000)), can indicate increased input of weathering products or changes in sediment provenance. In TTS ratios of some weathering sensitive elements to Ti increase after ~5 ka, e.g., Y/Ti ratios (Fig. 6d). Significantly, Y/Ti ratios in TTS have positive correlations with other more weathering sensitive element ratios, including Ca/Ti (r^2=0.7). They also show identical down-profile patterns to those of the highly weathering affected elements Sr and Rb (Kamber et al., 2005; Marx and Kamber, 2010) when those elements are also plotted as a ratio against Ti (note; both Sr and Rb contained too many zero counts to calculate meaningful correlations). Collectively, this implies the increase in Y/Ti at the top of the core is the result of weathering, either increased weathering itself, or increased transport of weathering products from the catchment, e.g. activation of hill slope material, both indicating increased precipitation and runoff at TTS.

5.2 Vegetation change and rainfall patterns inferred from stable isotopes

Stable carbon isotope ($\delta^{13}C_{TOC}$) analysis of organic matter can provide insight into plant species composition (e.g. C_3 v C_4), habitat and environmental stress (e.g. Boutton, 1996; Krull and Bray, 2005; Krull et al., 2004; Meyers and Ishiwatari, 1993; O'Leary, 1988; Stewart et al., 1995). Plants utilise C_3 ($\delta^{13}C$ -25 to -30‰) or C_4 ($\delta^{13}C$ -12 to -14‰) photosynthetic pathways to fractionate atmospheric CO_2 during the synthesis of organic compounds (O'Leary, 1988). These pathways can be differentiated from analysis of $\delta^{13}C$ in plants and associated organic matter. The range of $\delta^{13}C_{TOC}$ values in the TTS core imply a vegetation source of variable mixtures of C_3 and C_4 plants (Boutton 1996, Meyers and

Ishiwatari 1993) (Fig. 2c). This might be expected as the northern tropical savannas are composed of predominately of C_3 vegetation (trees) and grasses, which in tropical northern Australia are 90% C_4 (Hattersley, 1983), i.e., C_4 signatures have been identified in many northern Australia sedimentary deposits (e.g. Bird et al., 2019; Krull and Bray, 2005; Lloyd et al., 2008; Miller et al., 2018). The contribution of C_3 plants to the measured $\delta^{13}C_{TOC}$ can be quantified using Equation 2 (Ludlow et al., 1976);

$$C_3\,(\%) = (\delta^{13}C_{TOC} - \delta^{13}C_{C4}) / (\delta^{13}C_{C3} - \delta^{13}C_{C4}) \times 100 \quad (2)$$

where the $\delta^{13}C_{TOC}$, $\delta^{13}C_{C3}$, $\delta^{13}C_{C4}$ are $\delta^{13}C$ endmember values for C_3 woody plants (and grasses) and C_4 grasses, respectively.

C_3 estimates from older OM needs to consider other factors that influence $\delta^{13}C$ values. These include isotopic fractionation during soil organic matter (SOM) decomposition (e.g. Balesdent and Mariotti, 1996; Krull and Bray, 2005; Wang et al., 2008a), changes to atmospheric CO_2 concentrations ($[CO_2]_{atm}$), atmospheric $\delta^{13}C$ composition ($[\delta^{13}C]_{atm}$) and the effect of past rainfall regimes on $\delta^{13}C$ (Torres et al., 2020; Wang et al., 2008a). SOM decomposition results in the residual OM pool becoming enriched in $\delta^{13}C$. This effect ranges between 1‰ in arid and weakly developed soils, to 4‰ in wet tropical, well developed soils (Garten et al., 2000; Krull et al., 2006; Krull and Bray, 2005; Krull et al., 2002; Lehmann et al., 2002). Thus Equation 2 can be modified to include $\mathcal{E}$, the fractionation factor related to the extent of SOM decomposition.

$$C_3\,(\%) = (\delta^{13}C_{TOC} - \mathcal{E} - \delta^{13}C_{C4}) / (\delta^{13}C_{C3} - \delta^{13}C_{C4}) \times 100 \quad (3)$$

The endmember values for C_3 and C_4 for vegetation and $\mathcal{E}$ for TTS are described in the S1, alongside the corrections for changes to $[\delta^{13}C]_{atm}$ and $[CO_2]_{atm}$. Changes to MAP were estimated using the space for time substitution (see Section 2.8). As previously noted, there a number of assumptions involved in the space/time rainfall estimate, therefore ±20% was applied to the rainfall estimate, which is comparable with estimates of MAP based on $\delta^{15}N$ values (see below).

Three scenarios of modelled C_3 vegetation are presented; i) C_3 non-corrected data (using Eq. 2), ii) C_3 non-rainfall corrected data, which accounts for changing $[CO_2]_{atm}$, $[\delta^{13}C]_{atm}$, and decomposition ($\mathcal{E}$), and, iii) C_3 fully corrected data (Fig. 7g). C_3 fully corrected

data indicate C_3 vegetation contributed between 45-65% of TOC in TTS between 35 and 5 ka, after which C_3 increased to >75%. A noticeable increase in C_3 occurred around 25 ka from 40 to 60%, before a decline to 52% at ~15 ka. C_4 plants, with greater water use efficiency favour drier conditions and summer rainfall maxima, while C_3 prefer higher moisture availability and winter rainfall regimes (Cornwell et al., 2018; Ehleringer and Cerling, 2002). These relationships between photosynthetic type and moisture availability have been extensively used to infer past climates (e.g., Miller et al., 2018; Vidic and Montanez, 2004; Wynn and Bird, 2007).

Increasing C_3 between the Pleistocene and Holocene and the middle and late Holocene in TTS can therefore be interpreted as increasing moisture availability associated with enhanced IASM rainfall. The C_3 non-corrected and C_3 non-rainfall corrected estimates suggest C_3 was as low as 30% during the Pleistocene, reinforcing the important role of rainfall in influencing the $\delta^{13}C$ of C_3 vegetation (Stewart et al., 1995) and highlighting the need to correct for changing precipitation (Wang et al., 2008a). Although the estimate of precipitation change at TTS is uncertain, the difference between the C_3 fully corrected estimate and the C_3 non-rainfall corrected estimate provide a reasonable range of likelihood within which the percentage of C_3 vegetation could be expected to occur (Fig. 7g).

As well as catchment vegetation, other factors can influence $\delta^{13}C_{TOC}$ values, including freshwater algae and bacteria. Freshwater algae typically have $\delta^{13}C$ values of -26 to -30‰ (Meyers, 1997), similar to C_3 vegetation at TTS. To distinguish between algae and vegetation, C/N ratios are often used alongside $\delta^{13}C$ value (Lamb et al., 2006). This is possible as C/N ratios in algae are typically 4-10 where as they are >10 in C_3 vegetation (Lamb et al., 2006; Meyers, 1994).

The Pleistocene to Early Holocene aged sediments from TTS have $\delta^{13}C$ values lower than freshwater algae, but C/N ratios lower than terrestrial vegetation (Fig. 7d and g). This is consistent with microbial degradation of organic matter resulting in loss of C and gain of N (Benner et al., 1984; Meyers, 1994; Rice and Tenore, 1981; White and Howes, 1994). This limits ability to distinguish a terrestrial vegetation from that of algae in these sediments. A contribution of algae would therefore bias our results to C_3 vegetation before the Early Holocene, although algae in C_4 vegetation dominated catchments (e.g. in the Australian tropics) can record higher $\delta^{13}C$ values (<16‰) (Chivas et al., 2001). By contrast, Mid to Late-Holocene sediments in TTS exhibit C/N ratios >15 indicative of a dominantly C_3 vegetation signal. A contribution of algae

Analysis of $\delta^{15}N$ can provide further insight into shifting MAP at TTS. $\delta^{15}N$ values have previously been shown to respond to MAP, presumably because N consumers become more efficient with increasing moisture, lowering $\delta^{15}N$ values (Amundson et al., 2003; Austin and Vitousek, 1998). Bird et al., (2019) reported a negative relationship between MAP and $\delta^{15}N$ in lake sediments across the Top End. Applying that relationship to $\delta^{15}N$ values in the upper most samples in the TTS core resulted in a calculated MAP of 1780 mm (Root Mean Squared Error of Prediction (RMSEP) range = 2220-1350 mm/yr), matching measured MAP close to TTS (1940 mm/yr; 1993-2019 range = 2560-1320 mm/yr) (Fig. 7e). Therefore, $\delta^{15}N$ v values through the TTS core can be used to approximate palaeo precipitation. $\delta^{15}N$ values indicate MAP was below 1000 (range ~1400-400) mm/yr between 35 and 25 ka, increasing to >1500 mm/yr after 5 ka (Fig. 7e). This supports the interpretation of increased monsoonal rainfall for the later Holocene. It is noteworthy that the $\delta^{15}N$ predicted rainfall is within the range of MAP (albeit slightly higher) predicted using the space/time modelling approach.

$\delta^{13}C_{TOC}$ values of lake sediments across the Top End have a statistically significant positive relationship with the ratio of arboreal taxa to grass (Poaceae) (A/G) in lake sediment pollen (Bird et al., 2019). Thus, $\delta^{13}C_{TOC}$ values can be used to infer savanna woodiness at TTS. Applying the $\delta^{13}C_{TOC}$ to A/G relationship of Bird et al., (2019) to TTS $\delta^{13}C_{TOC}$ resulted in predicted A/G ratios of <5 in the Pleistocene section of the record and ~25 during the Holocene (Fig. 7f). These values overestimated measured A/G (from pollen) ratios by >40 times in the top of the TTS core. This is likely due to the effect of aquatic (C_3) plants (dominantly *Typha* spp.) that grow on swamp surface today and through much of the Holocene (Fig. 1c and 1d) increasing the $\delta^{13}C_{TOC}$ values above that of arboreal taxa alone. Alternatively, or additionally, changes in the proportion of C_3 grasses growing at TTS could also play a role.

Modelled TTS A/G ratios between 35 and 25 ka are ~1.5 (Fig. 7f). These equate to approximately 60% C_3 vegetation, similar to that calculated by Eq. 3. Modelled A/G ratios in TTS before 25 ka are similar to the A/G ratio obtained in (modern) surface pollen samples from lakes located between 0.5-1° south of TTS (i.e., near Katherine, ~250 km from the coastline). Vegetation at those latitudes is dominated by C_4 vegetation ($\delta^{13}C_{TOC}$ = ~-16 to -19; Bird et al., 2019), agian implying savanna at TTS was more C_4 grass dominated in the past.

During much of MIS2 the coastline was ~500 km from its present position (Yokoyama et al., 2001), however, estimated A/G ratios in TTS in MIS2 were similar to sites

250-30 km from the coastline today (Bird et al., 2019). That is, MAP was higher than predicted from the change in continentality alone. However, the relationship between $\delta^{13}C$ values and A/G ratios is not straightforward with A/G also likely influenced by a combination of other factors including fire regimes, soil texture, fertility and ground water (Bird et al., 2019; Hutley et al., 2011; Williams et al., 1996).

5.3 Palaeo-environments of the Top End since 35 ka

The record from TTS can be used to infer past environmental conditions at TTS, which are likely to reflect changes in water availability driven by changes to IASM activity. In the sections that follow, these changes are discussed within the four Zones identified from the geochronological structure of the TTS core (Fig.4). As noted, these broadly reflect the major boundaries of the late Quaternary. They are; *i)* Late MIS3 to early MIS2 (35-25 ka), *ii)* the LGM to Pleistocene/Holocene transition (25-10 ka), *iii)* the Early to Mid-Holocene (10-5 ka) and, *iv)* the Mid-Holocene to present. The demarcation of these zones is also supported by in other parameters within TTS, e.g stable isotopes, grainsize, geochemistry and pollen.

5.3.1 Late MIS3 to Early MIS2:

The shallow basin containing TTS began accumulating sediment from ~35 ka. Sediment deposited prior to 35 ka (Unit 6) was enriched in clay and Fe (Fig. 6b) consistent with weathered saprolite and indicating the onset of the lacustrine sediment deposition accumulation is contained within the studied core. This raises the question as to why TTS does not contain older sediment. Fluvial or aeolian erosion could have removed older sediment, with enhanced pluvial conditions, followed by increased aridity, recorded across northern Australia in MIS3 in the Gulf of Carpentaria, Kimberley (Reeves et al., 2008; Wende et al., 1997) and on the northern edge of Great Sandy Desert at Wolfe Creek and Lake Gregory (Fitzsimmons et al., 2012; Miller et al., 2018). Alternatively, structural changes (e.g. faulting) may have facilitated formation of the depression prior to 35 ka, although more data are needed to test this.

From ~35-25 ka alluvial sedimentation commenced in TTS. High Sr/Ca ratios indicate high evaporative concentration of salts, implying low moisture content (Fig. 6c). Similarly, low TOC, C/N, and Si/Ti (Fig. 6c and 7d) indicate minimal biological productivity, also suggesting limited moisture availability. Enriched $\delta^{15}N$ values suggest

MAP of <1000 mm/yr (Fig. 7e), while the lack of pollen preservation indicates highly oxidising conditions indicative of a largely dry basin.

Low water levels in TTS are also implied by high sand content before 25 ka. Given the prevalence of sandstone lithologies in the TTS catchment, sand is the dominant grainsize of hillslope sediments and swamp margin soils. Transport winnowing, as occurs when overland flow enters a water body is therefore required to deposit significant silt or clay in the centre of TTS. High sand content in TTS implies overland transport of sediment to the swamp centre, i.e., a reduced swamp water volume/extent (Fig. 6b).

Vegetation modelling indicated a greater proportion of C_4 was present (up to 60%), suggesting a more grass dominated savanna surrounding TTS (Fig. 7g). A slight decrease in $\delta^{15}N$ values combined with increasing silt content between 35-25 ka could indicate increased moisture at TTS within this period. Although this isn't easily resolvable in light of falling SL in late MIS3 (Grant et al., 2012) and is inconsistent with Australian records in general (Kemp et al., 2019), i.e., it requires further investigation.

Relatively dry conditions at TTS broadly match inferred conditions in the Gulf of Carpentaria, where a wetter early MIS3 transitioned to a dryer late MIS3 (Reeves et al., 2008). Similarly, at Wolfe Creek, ~740 km SW of TTS, a rapid decrease in water level occurred prior to 35 ka (Miller et al., 2018), while at Lake Gregory, ~860 km SW, increased dune building was interpreted to indicate relative aridity (Fitzsimmons et al., 2012).

These results indicate TTS had reduced functionality as a wetland before 25 ka, implying, by inference, that wetlands may have been limited across the Top End. Similarly, Top End savannas were more grass dominated, consisting of smaller trees and reduced species richness, likely resembling the composition of drier inland sites today (Williams et al., 1996). Overall, evidence from TTS indicates the IASM was significantly less effective before 25 ka, matching reduced monsoon strength recorded across the other major global monsoon systems in late MIS3 (Cruz et al., 2005; Gasse et al., 2008; Wang et al., 2008b; Weldeab et al., 2007).

5.3.2 The LGM to Pleistocene/Holocene transition:

Despite limited age control and evidence of geochronological complexity, TTS records increasing moisture availability after 25 ka, compared to 35-25 ka. This is shown by increasing Sr/Ti and Ca/K (Fig. 6c and d), implying greater in-swamp biological production, increased C_3 vegetation, potentially indicating a slightly greater abundance of woody

vegetation or aquatics, and greater silt deposition and reduced Sr/Ca, both indicating wetter conditions (Fig. 6c and 7g).

$\delta^{13}C_{TOC}$ values at TTS were similar to those inferred from Girraween Lagoon, Darwin, located 80 km north-east of TTS and one of few other Top End from this period (-16.1 versus -19‰, respectively) (Rowe et al., 2020). This implies a much higher abundance of C_4 vegetation, calculated to be ~50% at TTS. Unlike TTS, Girraween preserved a diverse pollen assemblage throughout the LGM to Holocene transition, including abundant poaceae, woody sclerophyll-monsoon forest, non-eucalyptus woody pollen and wetland pollen (Rowe et al., 2020). This diversity likely explains the approximately 50/50 C_3/C_4 vegetation mix modelled at TTS. The lack of pollen preservation at TTS, compared to nearby Girraween is likely attributable to local site factors, i.e., Girraween is a larger and deeper water body that retains water annually today, whereas TTS does not. Similar to TTS, Girraween recorded low fire activity (indicated by charcoal), but with more consistent presence/preservation.

Critically, evidence of continued/increasing moisture in the Top End at TTS and Girraween during the LGM contrasts with some northern Australia records which indicate enhanced aridity (e.g. Fitzsimmons et al., 2012; Kershaw et al., 2007; Kuhnt et al., 2015; Miller et al., 2018; Moss et al., 2017; Moss and Kershaw, 2000; Moss and Kershaw, 2007; Reeves et al., 2008; Wyrwoll and Miller, 2001). Increased moisture in the Top End is consistent with peak local insolation and increasing SST and sea level during late MIS2 (Fig. 7a). It is also consistent with other IASM records, which show pronounced millennial-scale variability during the LGM/MIS2. This includes speleothems from the Kimberley (Fig. 7c) (Denniston et al., 2017), Flores (Ayliffe et al., 2013) and Borneo (Partin et al., 2007), runoff records from Flores (Muller et al., 2012) and PNG (Shiau et al., 2011) and foraminifera patterns from a record off Java (Mohtadi et al., 2011).

Flores (Liang Luar cave) and Borneo speleothem records imply strengthening of the IASM between MIS3 and MIS2, similar to a *prima facie* interpretation of the TTS results. These, along with Kimberley speleothems, record wet intervals coinciding with Heinrich events, the Younger Dryas (YD) (and in the Kimberley a period termed the 'Late Glacial Pluvial' (LGP) at ~18.3/17.3 ka (Denniston et al., 2017) (Fig. 7c)), attributed to southward shifts in the IASM in response to North Atlantic cooling (Ayliffe et al., 2013). Modelling studies imply the seasonality of the IASM may have increased at the LGM, with enhanced early summer rain, but reduced annual rainfall (Yan et al., 2018), conditions which could

manifest in complex landscape and ecosystem responses. This could explain the apparent contradictions between the palaeoclimate records.

Despite possible hiatuses/unconformities in TTS between 25 and 10 ka, 391 mm of sediment accreted in the swamp. The sedimentation rate, which was the same as between 35–25 ka (~0.025 mm/yr), but lower than between 10-0 ka (0.046 mm/yr), demonstrates TTS was receiving sediment at least periodically during MIS 2. There is also evidence of increased sedimentation in Wangi plunge pool, directly below TTS, in mid to late MIS2 (May et al., 2015; Nott and Price, 1994).

Accretion of sediment in TTS may have occurred during the delglacial period (after 18 ka) when rapid marine transgression flooded of 2/3rds of Joseph Bonaparte Gulf (Yokoyama et al., 2001). This would have resulted in increased moisture advection to TTS, enhancing precipitation and alluvial deposition. This is supported by the Girraween Lagoon record which indicates increasing moisture after 12 ka (Rowe et al., 2020). It is also supported by the palaeo-hydrological model which indicates TTS would have experienced a 45% increase in swamp-full conditions between 18 and 12 ka (Fig. 5). Alternatively, or in conjunction, sediment accretion could have occurred during periodic (millennial-scale) wet events, as recorded in speleothems (Ayliffe et al., 2013; Denniston et al., 2017) and in runoff records (Muller et al., 2012; Shiau et al., 2011) during MIS2. Rapid changes in pollen type/diversity in Girraween Lagoon may also be indicative of these events (Rowe et al., 2020). Collectively this indicates phases of more active IASM activity occurred throughout MIS2, becoming frequent in deglacial period (Ayliffe et al., 2013; Denniston et al., 2017; Rowe et al., 2020).

Some marine records imply reduced runoff (drier conditions, or at least lower marine productivity) and weaker IASM activity during HS1, and the YD (Kuhnt et al., 2015; Mohtadi et al., 2011). This would constrain sediment accretion in TTS to either the LGM, the Bølling–Allerød (e.g. see Mohtadi et al., 2011) and/or after ~12 ka. A further possibility is that the majority of this sediment could have accreted after 14 ka when moisture availability and IASM activity increased across northern Australia (Field et al., 2017; Field et al., 2018c; Magee et al., 2004; Miller et al., 2018; Wyrwoll and Miller, 2001).

Possible sedimentation hiatuses/unconformities in TTS between 25 and 10 ka, combined with the low sedimentation rate, (Fig. 4) give rise to the possibility that sediment was removed by fluvial or aeolian activity during extended exposure of the TTS floor. Enhanced sedimentation in Wangi plunge pool during mid to late MIS2 (May et al., 2015;

Nott and Price, 1994) provides evidence of significant discharge, implying potential for sediment removal from TTS during intense run-off events, especially if the swamp was dry immediately beforehand.

In summary, TTS records increased moisture availability, indicative of at least periodic enhancement of the IASM, but also aridity between 25-10 ka. High monsoon variability during MIS2 also appears to be a feature of East Asian and Indian monsoons (Govil and Naidu, 2011; Wang et al., 2001; Wu et al., 2009). Variability in moisture availability at TTS is reflected in the complex age structure of the TTS core as indicated by the Ln/Tn DR_{norm} ratios. Similarly, C_3 estimates range from ~55-70%, implying millennial scale changes in ecosystem structure between more/less woody savanna (however $\delta^{15}N$ predicted rainfall displays little variability) (Fig. 7e-g). Episodic enhancement of IASM activity seems to have resulted in at least periodic establishment of a wetland at TTS, although the age structure of the core does not allow the timing of these periods to be established.

5.3.3 The Pleistocene/Holocene transition to Mid-Holocene:

By ~9 ka SL was close to its current position in Joseph Bonaparte Gulf (Yokoyama et al., 2001). This change coincides with an increase in C_3 vegetation, TOC and C/N ratios, the onset of pollen preservation and increasing charcoal in TTS (Fig. 8). This matches results from the proximal Gerriaween Lagoon, which also records continuous pollen preservation after 10 ka, (Rowe et al., 2019). These changes also match increased organic matter preservation in spring deposits across the Kimberley (Field et al., 2018a; Field et al., 2018c) and the return of rainforest taxa to northern Queensland (Moss et al., 2017). Collectively, this suggests wetlands became more permanent across northern Australia from 10 ka.

$\delta^{15}N$ values began to rapidly deplete at TTS after 10 ka, indicating MAP at TTS reached ~1500 mm by 5 ka (Fig. 7e). Pyrophobic vegetation, dominated by the fire-sensitive pine, *Callitris* sp., was abundant at TTS during the early Holocene, occurring coeval with low charcoal counts indicating low local fire activity (Fig. 8e and f). A wetter vegetation assemblage was similarly recorded at Girraween Lagoon in the early to Mid-Holocene (9-4 ka), with that site recoding standing water and peat production from 10 ka (Rowe et al., 2019). At both TTS and Girraween, a significant increase in charcoal after 10 ka matched increasing woody vegetation at both sites (Fig. 8g).

The increase in moisture indicated at TTS and Girraween also matches other local records of increased moisture. Namely, increased sedimentation in Wangi Plunge Pool (Nott and Price, 1994). Elsewhere across northern Australia increased moisture is also recorded in Kimberley Mound Springs (11-7.5 ka) (Field et al., 2018c) and by increased sedimentation in the Gilbert River, Gulf of Carpentaria (Nanson et al., 1991). Collectively this indicates increased IASM activity from 10-9 ka.

Increased *Typha* pollen (and aquatic pollen taxa more generally) in TTS toward the mid-Holocene (Fig. 8d) implies a further increase in effective moisture. This again matches with changes in the pollen assemblage Girraween Lagoon, suggesting enhanced wetland development (Rowe et al., 2019).

Typha is a key food plant for Aboriginal people and its greater abundance coincides with an overall growth of human populations in northern Australia after 9 ka, itself linked to an increase in resource availability in response to increased moisture (Williams et al., 2010; Williams et al., 2015). Increased anthropogenic management is likely also reflected in the decrease in abundance of pyrophobic trees and increase in pyrophilic trees and charcoal from the mid-Holocene (Fig. 8e and f). Although reduced IASM activity could also account for this effect, it isn't consistent with increasing aquatics and decreasing herbs (Fig. 8g).

While most biological information in TTS implies increasing moisture during the early Holocene, the ratio of Si/Ti decreases around the Pleistocene/Holocene transition (Fig. 6c), suggesting less in-swamp biological production and potentially drying. This broadly coincides with a reduction in C_3 vegetation, also indicative of dry conditions (note parametrisation of Equation 3 could account for this decrease, however), and reduced IASM activity recorded in Kimberley speleothems (Denniston et al., 2017). Whereas Kimberley speleothems indicate increased IASM activity from 9 ka and C_3 in TTS increases from 10 ka, matching the onset of increased pollen preservation in both TTS and in Girraween Lagoon (Rowe et al., 2019), the Si/Ti in does not increase again until after 5 ka. These discrepancies between proxies require further investigation, however, a possible explanation is that the change in Si/Ti at TTS could be driven by increased Ti input or non-climate factors affecting biological Si production (water chemistry, predation etc.).

Significantly, the onset of enhanced IASM conditions at TTS and at Girraween Lagoon postdate the precession forced changes to the major global monsoon systems from 14.8 ka (deMenocal et al., 2000). In addition, the onset of increased humidity in the Top End after 10 ka also contrasts with major drying events in African monsoon influenced lakes after 8 ka, (Gasse, 2000) and by the absence/retreat of glaciers from the monsoon influenced

catchments of the Central Andes between ~9-7 and at ~3 ka (Abbott et al., 2003). This suggests regional-scale changes in SL, insolation and land-sea heating may exert a more important control on IASM activity in the Top End by comparison to global-scale precessional forcing (e.g., see Marshall and Lynch, 2008; Yan et al., 2018). Although, Northern Hemisphere insolation is likely to still be an important boundary control on IASM strength in Australia (McRobie et al., 2015), i.e., there is evidence of a more minor increase in IASM activity from 14 ka (Field et al., 2018c).

Overall, the early to mid-Holocene in TTS and nearby Girraween Lagoon is marked by evidence of substantial change from ~10 ka (Fig. 6-8) indicating invigoration of the IASM. This coincides with increasing tropical insolation (Berger and Loutre, 1991; Laskar et al., 2004), SSTs in the IPWP (Stott et al., 2004) and increased La Nina-type conditions (Denniston et al., 2013b) and flooding of Joseph Bonaparte Gulf (Fig. 6a). These changes imply a southward shift/expansion of the ITCZ (Mariani et al., 2017; Marx et al., 2009). It is not possible to deconvolute these causes in the context of this study and they are unlikely to be independent, all would be expected to increase moisture in the Top End via enhanced IASM activity however.

5.3.4 Mid Holocene to present:

After 5 ka the pollen assemblage in TTS became indicative of a drier vegetation mosaic. Fire intolerant (pyrophobic) and aquatic plant taxa decreased while *Eucalyptus* pollen increased (Fig. 8e and f). These patterns are consistent with pollen records at other sites across northern Australia indicating drying from the mid-Holocene (Rowe et al., 2019; Shulmeister and Lees, 1995; Stevenson et al., 2015). At Girraween Lagoon declining grass and increasing charcoal and Eucalypt pollen occurred from 4 ka, with Eucalypt pollen peaking at 3-0.6 ka (Rowe et al., 2019). Collectively this implies local drying within the wetlands of the Top End. Similarly, in the Kimberley, dry conditions occurred from 7.5 ka, intensifying further after 4 ka (Field et al., 2017; Field et al., 2018c). These changes also coincide with increased dust transport from central Australia (Marx et al., 2009), including enhanced dust deposition in the Kimberley (Fig. 8b) (McGowan et al., 2012), broadly attributed to increased El Niño-type climate variability (Marx et al., 2009) which is associated with contemporary IASM suppression (Evans and Allan, 1992; Lau and Nath, 2000).

While pollen and charcoal indicate drying at TTS after 5 ka, TOC and C/N increased rapidly, indicating better preservation conditions (Fig. 7d) indicative of increased moisture. Similarly, $\delta^{15}N$ values imply rainfall increased, approaching modern MAP in the late Holocene, as indicated by the top most samples in the TTS core. Sand content in TTS also increased in the mid to late Holocene, again particularly in the top of core, indicative of increased velocity of overland flow due to increased rainfall (Fig. 6b /8c). Further evidence of increased moisture is provided by increased deposition of weathering products after 5 ka (Fig. 6d/8c).

C_3 vegetation also increased to its highest percentage after 5 ka (~80%). This is consistent with a more woody savanna, suggesting the savanna surrounding TTS approached its modern composition from that time. For example, $\delta^{13}C$ values in TTS after 5 ka are similar to modern leaf litter (when corrected for soil decomposition).

Although increased C_3 vegetation after 5 ka could be partly driven by *Typha* growth in the swamp, *Typha* and total aquatics decrease in the top of the core as does total arboreal taxa (Fig. 8d and g). Grass, herbs and Pteridophytes increase, implying C_3 varieties of these vegetation types contributed to the increase in C_3 recorded in TTS. As C_3 grasses and Pteridophytes are more likely mesic (Hattersley, 1983; Kotze and O'Connor, 2000), periodic/seasonal changes in swamp persistent/extent could result in their enhanced growth in and around the swamp. Alternatively, or in addition, increased human populations in the mid to late Holocene in northern tropical Australia (especially after 2 ka) (Williams et al., 2010; Williams et al., 2015) could have contributed to ecosystem change both around TTS itself and more broadly across the Top End.

It is difficult to resolve the timing of changes in TTS below <5 kys BP. However, the evidence of increased moisture in the late Holocene at TTS occurs coincident with increased moisture in the late Holocene at Girraween Lagoon (Rowe et al., 2019). Similarly, the increase in savanna woodiness recorded at TTS in the late Holocene is also evident at Girraween. Alongside this, increased discharge was recorded in Kimberley springs in the Late Holocene (at ~3-2 ka) (McGowan et al., 2012), while runoff to the Timor Sea/Indian Ocean also increased(Kuhnt et al., 2015) (Fig. 7b and 8b), implying increased moisture across northern Australia. It should be noted, however, that the Kimberly springs records are complex, with pollen and other evidence also indicating late Holocene drying (Field et al., 2017; Field et al., 2018c).

Within the wider IASM region, increased IASM strength in the late Holocene is recorded across Indonesia, including south of Java from 2.5 ka (Mohtadi et al., 2011), Sumba from 2.8 ka (Steinke et al., 2014) and at Flores and Borneo from 3 ka (Griffiths et al., 2010; Partin et al., 2007). Stronger IASM activity in the late Holocene is also coincident with increased activity of both the African (Gasse, 2000) and South American monsoons (Abbott et al., 2003; Hooper et al., 2020).

Overall IASM activity over the late Holocene remains somewhat uncertain. While pollen in TTS indicates a general drying, there is also evidence of wetter conditions. This apparently contradictory evidence could imply high variability in IASM conditions, consistent with increased ENSO activity 5-2 ka, with a potentially stronger but still variable IASM after that time, or the influence of increased human activity, or both. Despite this, the TTS wetland remained broadly established after 5 ka, albeit experiencing variable conditions, while the surrounding savanna also established its current configuration from this time.

6.0 Conclusions

Table Top Swamp contains a semi-continuous palaeo-environmental record since 35 ka. Despite the geochronological complexity of the studied core a number of distinctive time zones are identifiable in TTS. Results indicated a more grassy savanna existed in the Top End between 35 and 25 ka, with C_4 vegetation contributing around 50% of organic C by comparison to 20% today. The TTS was less established, indicating a significantly subdued IASM and suggesting wetlands were more limited across the Top End. Between 25 and 10 ka humidity increased at TTS, as indicated by increased in-swamp production, increased C_3 vegetation and greater lacustrine winnowing of grainsize, confirming at least periodic establishment of swampy conditions. Luminescence data suggest a number of hiatuses/unconformities in sedimentation occurred during this period which likely reflect pronounced shifts in IASM activity as recorded in other Australian and Indonesian studies. Constraining the timing of these shifts remains an important challenge for understanding IASM dynamics and ecosystem change and resilience in tropical Australia.

A dramatic shift in climate and ecosystems was recorded from ~10 ka associated with an approximately 50% increase in water availability. This included the onset of pollen preservation, an increase in TOC and C/N, and a shift to a more woody dominated savanna. This points to invigoration of the IASM, corresponding with establishment of a seasonally

active wetland at TTS, with $\delta^{15}N$ implying rainfall reached modern levels from this time. Results from TTS and combined with those from elsewhere across northern Australia (e.g., in Girraween Lagoon (Rowe et al., 2019) and in mounds springs from the Kimberly (Field et al., 2017; Field et al., 2018c)) indicate the current configuration of ecosystems across the Top End likely broadly date from this time. Significantly, invigoration of the IASM in the Top End occurred later than the precession-forced response recorded in other global monsoon system. This implies moisture proximity (i.e., the coastline position) and other regional-scale factors are key controls on IASM effectiveness in northern Australia.

A shift from wetter, less fire-prone, vegetation to drier vegetation and increased charcoal occurred at ~5 ka. However, this was also accompanied by evidence of greater rainfall, increased C_3 vegetation and the delivery of more weathered sediment to TTS, all indicating increased humidity. These contrasting conditions could indicate increased IASM variability, i.e., ENSO activity increased after ~5 ka. Alternatively, the increasing presence of humans in the landscape may have facilitated a decoupling between vegetation and climate, for example through greater use of fire.

Acknowledgements

This study was funded by an ARC Discovery Early Career Research Award (DP0987819) granted to JHM. We also acknowledge financial support from the Australian Government for the Centre for Accelerator Science at ANSTO through the National Collaborative Research Infrastructure Strategy (NCRIS) and from the GeoQuEST Research Centre, The University of Wollongong. The authors would like to thank the Litchfield National Park team for granting access to TTS and providing valuable logistical support. We also think two anonymous Reviewers for their constructive and thoughtful comments.

References

Abbott, M.B., Wolfe, B.B., Wolfe, A.P., Seltzer, G.O., Aravena, R., Mark, B.G., Polissar, P.J., Rodbell, D.T., Rowe, H.D. and Vuille, M. (2003) Holocene paleohydrology and glacial history of the central Andes using multiproxy lake sediment studies. Palaeogeography, Palaeoclimatology, Palaeoecology 194, 123-138.

Ahmad, M. and Hollis, J.A. (2013) Chapter 5: Pine Creek Orogen, in: Ahmad, M., Munson, T.J. (Eds.), Geology and mineral resources of the Northern Territory Northern Territory Geological Survey, p. 133.

Ahmad, M., Wygralak, A.S., Ferenczi, P.A. and Bajwah, Z.U. (1993) Explanatory notes andmineral deposit data sheets - pine Creek SD 52-8.

Amundson, R., Austin, A.T., Schuur, E.A.G., Yoo, K., Matzek, V., Kendall, C., Uebersax, A., Brenner, D. and Baisden, W.T. (2003) Global patterns of the isotopic composition of soil and plant nitrogen. Global Biogeochemical Cycles 17, n/a-n/a.

Austin, A. and Vitousek, P.M. (1998) Nutrient dynamics on a precipitation gradient. Oecologia 113, 519-529.

Ayliffe, L.K., Gagan, M.K., Zhao, J.-x., Drysdale, R.N., Hellstrom, J.C., Hantoro, W.S., Griffiths, M.L., Scott-Gagan, H., Pierre, E.S., Cowley, J.A. and Suwargadi, B.W. (2013) Rapid interhemispheric climate links via the Australasian monsoon during the last deglaciation. Nature Communications 4, 2908.

Babechuk, M.G., Widdowson, M., Murphy, M. and Kamber, B.S. (2015) A combined Y/Ho, high field strength element (HFSE) and Nd isotope perspective on basalt weathering, Deccan Traps, India. Chemical Geology 396, 25-41.

Balesdent, J. and Mariotti, A. (1996) Measurement of soil organic matter turnover using 13C natural abundance. In ', in: TW Boutton, T.W., Yamasaki, S. (Ed.), Mass spectrometry of soils. Marcel Dekker Inc., New York, pp. 83-111.

Benner, R., Newell, S.Y., Maccubbin, A.E. and Hodson, R.E. (1984) Relative contributions of bacteria and fungi to rates of degradation of lignocellulosic detritus in salt-marsh sediments. Appl Environ Microbiol 48, 36-40.

Berger, A. and Loutre, M.F. (1991) Insolation values for the climate of the last 10 million years. Quaternary Science Reviews 10, 297-317.

Beringer, J., Hutley, L.B., Abramson, D., Arndt, S.K., Briggs, P., Bristow, M., Canadell, J.G., Cernusak, L.A., Eamus, D., Edwards, A.C., Evans, B.J., Fest, B., Goergen, K., Grover, S.P., Hacker, J., Haverd, V., Kanniah, K., Livesley, S.J., Lynch, A., Maier, S., Moore, C., Raupach, M., Russell-Smith, J., Scheiter, S., Tapper, N.J. and Uotila, P. (2015) Fire in Australian savannas: from leaf to landscape. Global Change Biology 21, 62-81.

Bird, M.I., Brand, M., Diefendorf, A.F., Haig, J.L., Hutley, L.B., Levchenko, V., Ridd, P.V., Rowe, C., Whinney, J., Wurster, C.M. and Zwart, C. (2019) Identifying the 'savanna' signature in lacustrine sediments in northern Australia. Quaternary Science Reviews 203, 233-247.

Boutton, T.W. (1996) Stable carbon isotope ratios of soil organic matter and their use as indicators of vegetation and climate change, in: Boutton, T.W., Yamasaki, S.I., (Ed.), Mass spectrometry of soils. Marcel-Dekker, New York, U.S.A.

Bowman, D.M.J.S., Brown, G.K., Braby, M.F., Brown, J.R., Cook, L.G., Crisp, M.D., Ford, F., Haberle, S., Hughes, J., Isagi, Y., Joseph, L., McBride, J., Nelson, G. and Ladiges, P.Y. (2010a) Biogeography of the Australian monsoon tropics. Journal of Biogeography 37, 201-216.

Bowman, D.M.J.S., Murphy, B.P. and Banfai, D.S. (2010b) Has global environmental change caused monsoon rainforests to expand in the Australian monsoon tropics? Landscape Ecology 25, 1247-1260.

Brown, E.T. (2015) Estimation of Biogenic Silica Concentrations Using Scanning XRF: Insights from Studies of Lake Malawi Sediments, in: Croudace, I.W., Rothwell, R.G. (Eds.), Micro-XRF Studies of Sediment Cores: Applications of a non-destructive tool for the environmental sciences. Springer Netherlands, Dordrecht, pp. 267-277.

Brown, E.T., Johnson, T.C., Scholz, C.A., Cohen, A.S. and King, J.W. (2007) Abrupt change in tropical African climate linked to the bipolar seesaw over the past 55,000 years. Geophysical Research Letters 34.

Chen, F.-H., Shi, Q. and Wang, J.-M. (1999) Environmental changes documented by sedimentation of Lake Yiema in arid China since the late Glaciation. Journal of Paleolimnology 22, 159-169.

Chivas, A.R., García, A., van der Kaars, S., Couapel, M.J.J., Holt, S., Reeves, J.M., Wheeler, D.J., Switzer, A.D., Murray-Wallace, C.V., Banerjee, D., Price, D.M., Wang, S.X., Pearson, G., Edgar, N.T., Beaufort, L., De Deckker, P., Lawson, E. and Cecil, C.B.

(2001) Sea-level and environmental changes since the last interglacial in the Gulf of Carpentaria, Australia: an overview. Quaternary International 83–85, 19-46.

Cook, G.D. and Heerdegen, R.G. (2001) Spatial variation in the duration of the rainy season in monsoonal Australia. International Journal of Climatology 21, 1723-1732.

Cornwell, W.K., Cornelissen, J.H.C., Turner, J., Wright, I.J., Maire, V., Barbour, M.M., Keitel, C., Cernusak, L.A., Dawson, T., Ellsworth, D., Reich, P.B., Farquhar, G.D., Griffiths, H., Knohl, A., Williams, D.G., Bhaskar, R., Richards, A., Schmidt, S., Valladares, F., Körner, C., Schulze, E.D., Buchmann, N. and Santiago, L.S. (2018) Climate and soils together regulate photosynthetic carbon isotope discrimination within C3 plants worldwide. Global Ecology and Biogeography 27, 1056-1067.

Croudace, I.W. and Rothwell, R.G. (2015) Micro-XRF Studies of Sediment Cores: Applications of a non-destructive tool for the environmental sciences. Springer.

Cruz, F.W., Burns, S.J., Karmann, I., Sharp, W.D., Vuille, M., Cardoso, A.O., Ferrari, J.A., Silva Dias, P.L. and Viana, O. (2005) Insolation-driven changes in atmospheric circulation over the past 116,000 years in subtropical Brazil. Nature 434, 63-66.

Davies, S.J., Lamb, H.F. and Roberts, S.J. (2015) Micro-XRF Core Scanning in Palaeolimnology: Recent Developments, in: Croudace, I.W., Rothwell, R.G. (Eds.), Micro-XRF Studies of Sediment Cores: Applications of a non-destructive tool for the environmental sciences. Springer Netherlands, Dordrecht, pp. 189-226.

deMenocal, P., Ortiz, J., Guilderson, T., Adkins, J., Sarnthein, M., Baker, L. and Yarusinsky, M. (2000) Abrupt onset and termination of the African Humid Period:: rapid climate responses to gradual insolation forcing. Quaternary Science Reviews 19, 347-361.

Denniston, R.F., Asmerom, Y., Polyak, V.J., Wanamaker, A.D., Ummenhofer, C.C., Humphreys, W.F., Cugley, J., Woods, D. and Lucker, S. (2017) Decoupling of monsoon activity across the northern and southern Indo-Pacific during the Late Glacial. Quaternary Science Reviews 176, 101-105.

Denniston, R.F., Wyrwoll, K.-H., Asmerom, Y., Polyak, V.J., Humphreys, W.F., Cugley, J., Woods, D., LaPointe, Z., Peota, J. and Greaves, E. (2013a) North Atlantic forcing of millennial-scale Indo-Australian monsoon dynamics during the Last Glacial period. Quaternary Science Reviews 72, 159-168.

Denniston, R.F., Wyrwoll, K.-H., Polyak, V.J., Brown, J.R., Asmerom, Y., Wanamaker, A.D., LaPointe, Z., Ellerbroek, R., Barthelmes, M., Cleary, D., Cugley, J., Woods, D. and Humphreys, W.F. (2013b) A Stalagmite record of Holocene Indonesian–Australian summer monsoon variability from the Australian tropics. Quaternary Science Reviews 78, 155-168.

Ehleringer, J.R. and Cerling, T.E. (2002) C_3 and C_4 Photosynthesis, in: Mooney, H.A., Canadell, J.G. (Eds.), Encyclopedia of Global Environmental Change. John Wiley and Sons, Ltd., Chichester, England, pp. 186 - 190.

Eroglu, D., McRobie, F.H., Ozken, I., Stemler, T., Wyrwoll, K.-H., Breitenbach, S.F.M., Marwan, N. and Kurths, J. (2016) See–saw relationship of the Holocene East Asian–Australian summer monsoon. Nature Communications 7, 12929.

Evans, J.L. and Allan, R.J. (1992) El Nino/southern oscillation modification to the structure of the monsoon and tropical cyclone activity in the Australasian region. International Journal of Climatology 12, 611-623.

Fensham, R.J., Fairfax, R.J. and Ward, D.P. (2009) Drought-induced tree death in savanna. Global Change Biology 15, 380-387.

Fensham, R.J., Low Choy, S.J., Fairfax, R.J. and Cavallaro, P.C. (2003) Modelling trends in woody vegetation structure in semi-arid Australia as determined from aerial photography. Journal of Environmental Management 68, 421-436.

Field, E., Marx, S., Haig, J., May, J.-H., Jacobsen, G., Zawadzki, A., Child, D., Heijnis, H., Hotchkis, M., McGowan, H. and Moss, P. (2018a) Untangling geochronological complexity in organic spring deposits using multiple dating methods. Quaternary Geochronology 43, 50-71.

Field, E., Marx, S., Haig, J., May, J.H., Jacobsen, G., Zawadzki, A., Child, D., Heijnis, H., Hotchkis, M., McGowan, H. and Moss, P. (2018b) Untangling geochronological complexity in organic spring deposits using multiple dating methods. Quaternary Geochronology 43, 50-71.

Field, E., McGowan, H., A., Moss, P.T. and Marx, S.K. (2017) A late Quaternary record of monsoon variability in the northwest Kimberley, Australia. Quaternary International In Press.

Field, E., Tyler, J., Gadd, P.S., Moss, P., McGowan, H. and Marx, S. (2018c) Coherent patterns of environmental change at multiple organic spring sites in northwest Australia: Evidence of Indonesian-Australian summer monsoon variability over the last 14,500 years. Quaternary Science Reviews 196, 193-216.

Fitzsimmons, K.E., Miller, G.H., Spooner, N.A. and Magee, J.W. (2012) Aridity in the monsoon zone as indicated by desert dune formation in the gregory lakes basin, northwestern Australia. Australian Journal of Earth Sciences 59, 469-478.

Forbes, M., Jankowski, N., Cohen, T., Hopf, F., Mueller, D., Bird, M., Haberle, S. and Jacobs, Z. (2020) Palaeochannels of Australia's Riverine Plain - Reconstructing past vegetation environments across the Late Pleistocene and Holocene. Palaeogeography, Palaeoclimatology, Palaeoecology 545, 109533.

Fu, J.C. and Koutras, M.V. (1994) Distribution Theory of Runs: A Markov Chain Approach. Journal of the American Statistical Association 89, 1050-1058.

Garten, C.T.J., Cooper, L.W., Post III, W.M. and Hanson, P.J. (2000) Climate controls on forest soil C isotope ratios in the Southern Appalachian Mountains. Ecology 81, 1108-1119.

Gasse, F. (2000) Hydrological changes in the African tropics since the Last Glacial Maximum. Quaternary Science Reviews 19, 189-211.

Gasse, F., Chalié, F., Vincens, A., Williams, M.A.J. and Williamson, D. (2008) Climatic patterns in equatorial and southern Africa from 30,000 to 10,000 years ago reconstructed from terrestrial and near-shore proxy data. Quaternary Science Reviews 27, 2316-2340.

Gerhart, L.M. and Ward, J.K. (2010) Plant responses to low [CO2] of the past. New Phytologist 188, 674-695.

Govil, P. and Naidu, P.D. (2011) Variations of Indian monsoon precipitation during the last 32kyr reflected in the surface hydrography of the Western Bay of Bengal. Quaternary Science Reviews 30, 3871-3879.

Grant, K.M., Rohling, E.J., Bar-Matthews, M., Ayalon, A., Medina-Elizalde, M., Ramsey, C.B., Satow, C. and Roberts, A.P. (2012) Rapid coupling between ice volume and polar temperature over the past 150,000 years. Nature 491, 744-747.

Griffiths, M.L., Drysdale, R.N., Gagan, M.K., Frisia, S., Zhao, J.-x., Ayliffe, L.K., Hantoro, W.S., Hellstrom, J.C., Fischer, M.J., Feng, Y.-X. and Suwargadi, B.W. (2010) Evidence for Holocene changes in Australian–Indonesian monsoon rainfall from stalagmite trace element and stable isotope ratios. Earth and Planetary Science Letters 292, 27-38.

Grosjean, M., van Leeuwen, J.F.N., van der Knaap, W.O., Geyh, M.A., Ammann, B., Tanner, W., Messerli, B., Núñez, L.A., Valero-Garcés, B.L. and Veit, H. (2001) A 22,000 14C year BP sediment and pollen record of climate change from Laguna Miscanti (23°S), northern Chile. Global and Planetary Change 28, 35-51.

Hattersley, P.W. (1983) The Distribution of C3 and C4 grasses in Australia in relation to climate. Oecologia 57, 113-128.

Heiri, O., Lotter, A.F. and Lemcke, G. (2001) Loss on ignition as a method for estimating organic and carbonate content in sediments: reproducibility and comparability of results. Journal of Paleolimnology 25, 101-110.

Hill, I.G., Worden, R.H. and Meighan, I.G. (2000) Yttrium: The immobility-mobility transition during basaltic weathering. Geology 28, 923-926.

Hill, M.J. and Hanan, N.P. (2010) Ecosystem Function in Savannas : Measurement and Modeling at Landscape to Global Scales. CRC Press LLC, Baton Rouge, UNITED STATES.

Hollis, J.A. and Glass, L. (2011) 1:250 000 geological map series, SD 52-08, in: In: Survey, N.T.G.E., Pine Creek, Northern Territory, Darwin. (Ed.)

Hooper, J., Marx, S.K., May, J.-H., Lupo, L.C., Kulemeyer, J.J., Pereira, E.d.l.Á., Seki, O., Heijnis, H., Child, D., Gadd, P. and Zawadzki, A. (2020) Dust deposition tracks late-Holocene shifts in monsoon activity and the increasing role of human disturbance in the Puna-Altiplano, northwest Argentina. The Holocene 30, 519-536.

Hutley, L.B., Beringer, J., Isaac, P.R., Hacker, J.M. and Cernusak, L.A. (2011) A sub-continental scale living laboratory: Spatial patterns of savanna vegetation over a rainfall gradient in northern Australia. Agricultural and Forest Meteorology 151, 1417-1428.

Ishiwa, T., Yokoyama, Y., Reuning, L., McHugh, C.M., De Vleeschouwer, D. and Gallagher, S.J. (2019) Australian Summer Monsoon variability in the past 14,000 years revealed by IODP Expedition 356 sediments. Progress in Earth and Planetary Science 6, 17.

Jackson, S., Storrs, M. and Morrison, J. (2005) Recognition of Aboriginal rights, interests and values in river research and management: Perspectives from northern Australia. Ecological Management & Restoration 6, 105-110.

Johnson, B.J., Miller, G.H., Fogel, M.L., Magee, J.W., Gagan, M.K. and Chivas, A.R. (1999) 65,000 Years of Vegetation Change in Central Australia and the Australian Summer Monsoon. Science 284, 1150-1152.

Jourdain, N.C., Gupta, A.S., Taschetto, A.S., Ummenhofer, C.C., Moise, A.F. and Ashok, K. (2013) The Indo-Australian monsoon and its relationship to ENSO and IOD in reanalysis data and the CMIP3/CMIP5 simulations. Climate Dynamics 41, 3073-3102.

Kajikawa, Y., Wang, B. and Yang, J. (2010) A multi-time scale Australian monsoon index. International Journal of Climatology 30, 1114-1120.

Kamber, B.S., Greig, A. and Collerson, K.D. (2005) A new estimate for the composition of weathered young upper continental crust from alluvial sediments, Queensland, Australia. Geochimica Et Cosmochimica Acta 69, 1041-1058.

Kemp, C.W., Tibby, J., Arnold, L.J. and Barr, C. (2019) Australian hydroclimate during Marine Isotope Stage 3: A synthesis and review. Quaternary Science Reviews 204, 94-104.

Kershaw, A.P., Bretherton, S.C. and van der Kaars, S. (2007) A complete pollen record of the last 230 ka from Lynch's Crater, north-eastem Australia. Palaeogeography Palaeoclimatology Palaeoecology 251, 23-45.

Kirkpatrick, J., Bowman, D., Wilson, B. and Dickinson, K. (1987) A transect study of the Eucalyptus forests and woodlands of a dissected sandstone and laterite plateau near Darwin, Northern territory, vol. 12, pp. 339-59. Australian Journal of Ecology 12, 339-359.

Knighton, A.D. and Nanson, G.C. (2001) An event-based approach to the hydrology of arid zone rivers in the Channel Country of Australia. Journal of Hydrology 254, 102-123.

Kotze, D.C. and O'Connor, T.G. (2000) Vegetation variation within and among palustrine wetlands along an altitudinal gradient in KwaZulu-Natal, South Africa. Plant Ecology 146, 77-96.

Krull, E., Haynes, D., Lamontagne, S., Gell, P., McKirdy, D., Hancock, G., McGowan, J. and Smernik, R. (2009) Changes in the chemistry of sedimentary organic matter within the Coorong over space and time. Biogeochemistry, 1-17.

Krull, E.G. and Bray, S.S. (2005) Assessment of vegetation change and landscape variability by using stable carbon isotopes of soil organic matter. Australian Journal of Botany 53, 651-661.

Krull, E.S., Bestland, E.A. and Gates, W.P. (2002) Soil organic matter decomposition and turnover in a tropical Ultisol: Evidence from δ13C, δ15N and geochemistry. Radiocarbon 44, 93-112.

Krull, E.S., Skjemstad, J.O. and Thompso, C.H. (2004) Chemistry, radiocarbon ages, and development of a subtropical acid peat in Queensland, Australia. Australian Journal of Soil Research 42, 411-425.

Kuhnt, W., Holbourn, A., Xu, J., Opdyke, B., De Deckker, P., Röhl, U. and Mudelsee, M. (2015) Southern Hemisphere control on Australian monsoon variability during the late deglaciation and Holocene. Nature Communications 6, 5916.

Kylander, M.E., Ampel, L., Wohlfarth, B. and Veres, D. (2011) High-resolution X-ray fluorescence core scanning analysis of Les Echets (France) sedimentary sequence: new insights from chemical proxies. Journal of Quaternary Science 26, 109-117.

Lamb, A.L., Wilson, G.P. and Leng, M.J. (2006) A review of coastal palaeoclimate and relative sea-level reconstructions using δ13C and C/N ratios in organic material. Earth-Science Reviews 75, 29-57.

Laskar, J., Robutel, P., Joutel, F., Gastineau, M., Correia, A.C.M. and Levrard, B. (2004) A long-term numerical solution for the insolation quantities of the Earth. A&A 428, 261-285.

Lau, N.-C. and Nath, M.J. (2000) Impact of ENSO on the Variability of the Asian–Australian Monsoons as Simulated in GCM Experiments. Journal of Climate 13, 4287-4309.

Lauterbach, S., Brauer, A., Andersen, N., Danielopol, D.L., Dulski, P., Hüls, M., Milecka, K., Namiotko, T., Obremska, M., Von Grafenstein, U. and Participants, D. (2011) Environmental responses to Lateglacial climatic fluctuations recorded in the sediments of pre-Alpine Lake Mondsee (northeastern Alps). Journal of Quaternary Science 26, 253-267.

Lehmann, M.F., Bernasconi, S.M., McKenzie, J.A. and Barbieri, A. (2002) Preservation of organic matter and alteration of its carbon and nitrogen isotope composition

during simulated and in situ early sedimentary diagenesis. Geochimica et Cosmochimica Acta 66, 3573-3584.

Liu, Z., Otto-Bliesner, B., Kutzbach, J., Li, L. and Shields, C. (2003) Coupled Climate Simulation of the Evolution of Global Monsoons in the Holocene. Journal of Climate 16, 2472-2490.

Lloyd, J., Bird, M.I., Vellen, L., Miranda, A.C., Veenendaal, E.M., Djagbletey, G., Miranda, H.S., Cook, G. and Farquhar, G.D. (2008) Contributions of woody and herbaceous vegetation to tropical savanna ecosystem productivity: a quasi-global estimate†. Tree Physiology 28, 451-468.

Löwemark, L., Chen, H.F., Yang, T.N., Kylander, M., Yu, E.F., Hsu, Y.W., Lee, T.Q., Song, S.R. and Jarvis, S. (2011) Normalizing XRF-scanner data: A cautionary note on the interpretation of high-resolution records from organic-rich lakes. Journal of Asian Earth Sciences 40, 1250-1256.

Ludlow, M.M., Troughton, J.H. and Jones, R.J. (1976) A technique to determine the percentage of C3 and C4 species in plant samples using stable natural isotopes of carbon. J. Ag. Sci. 87, 625-632.

Magee, J.W., Miller, G.H., Spooner, N.A. and Questiaux, D. (2004) Continuous 150 k.y. monsoon record from Lake Eyre, Australia: Insolation-forcing implications and unexpected Holocene failure. Geology 32, 885-888.

Mariani, M., Fletcher, M.-S., Drysdale, R.N., Saunders, K.M., Heijnis, H., Jacobsen, G. and Zawadzki, A. (2017) Coupling of the Intertropical Convergence Zone and Southern Hemisphere mid-latitude climate during the early to mid-Holocene. Geology 45, 1083-1086.

Marshall, A.G. and Lynch, A.H. (2008) The sensitivity of the Australian summer monsoon to climate forcing during the late Quaternary. Journal of Geophysical Research: Atmospheres 113.

Marx, S.K. and Kamber, B.S. (2010) High-precision trace-element systematics of sediments in the Murray-Darling Basin, Australia: sediment tracing and palaeo-climate implications of fine scale chemical heterogeneity of the upper continental crust. Applied Geochemistry 25, 1221-1237.

Marx, S.K., McGowan, H.A. and Kamber, B.S. (2009) Long-range dust transport from eastern Australia: a proxy for Holocene aridity and ENSO-induced climate variability. Earth and Planetary Science Letters 282, 167-177.

May, J.H., Marx, S.K., Reynolds, W.J., Clarke-Balzan, L., Jacobson, G. and Preusser, F. (2018) Establishing a chronological framework for a late Quaternary seasonal swamp in the Australian 'Top End'. Quaternary Geochronology 47, 81-92.

May, J.H., Preusser, F. and Gliganic, L.A. (2015) Refining late Quaternary plunge pool chronologies in Australia's monsoonal 'Top End'. Quaternary Geochronology 30, 328-333.

Mazumder, D., Iles, J., Kelleway, J., Kobayashi, T., Knowles, L., Saintilan, N. and Hollins, S. (2010) Effect of acidification on elemental and isotopic compositions of sediment organic matter and macro-invertebrate muscle tissues in food web research. Rapid Communications In Mass Spectrometry: RCM 24, 2938-2942.

McGowan, H., A., Marx, S.K., Moss, P. and Hammond, A.P. (2012) Evidence of ENSO mega-drought triggered collapse of prehistory Aboriginal society in northwest Australia. Geophysical Research Letters 39, L22702.

McRobie, F.H., Stemler, T. and Wyrwoll, K.H. (2015) Transient coupling relationships of the Holocene Australian monsoon. Quaternary Science Reviews 121, 120-131.

Meyers, P.A. (1994) Preservation of elemental and isotopic source identification of sedimentary organic matter. Chemical Geology 114, 289-302.

Meyers, P.A. (1997) Organic geochemical proxies of paleoceanographic, paleolimnologic, and paleoclimatic processes. Organic Geochemistry 27, 213-250.

Meyers, P.A. and Ishiwatari, R. (1993) Lacustrine organic geochemistry-an overview of indicators of organic matter sources and diagenesis in lake sediments. Organic Geochemistry 20, 867-900.

Miller, G., Mangan, J., Pollard, D., Thompson, S., Felzer, B. and Magee, J. (2005) Sensitivity of the Australian Monsoon to insolation and vegetation: Implications for human impact on continental moisture balance. Geology 33, 65-68.

Miller, G.H., Magee, J.W., Fogel, M.L., Wooller, M.J., Hesse, P.P., Spooner, N.A., Johnson, B.J. and Wallis, L. (2018) Wolfe Creek Crater: A continuous sediment fill in the Australian Arid Zone records changes in monsoon strength through the Late Quaternary. Quaternary Science Reviews 199, 108-125.

Mohtadi, M., Oppo, D.W., Steinke, S., Stuut, J.-B.W., De Pol-Holz, R., Hebbeln, D. and Lückge, A. (2011) Glacial to Holocene swings of the Australian–Indonesian monsoon. Nature Geoscience 4, 540-544.

Montanari, L., Sivapalan, M. and Montanari, A. (2006) Investigation of dominant hydrological processes in a tropical catchment in a monsoonal climate via the downward approach. Hydrology & Earth System Sciences 10, 769-782.

Moore, C.E., Beringer, J., Donohue, R.J., Evans, B., Exbrayat, J.-F., Hutley, L.B. and Tapper, N.J. (2018) Seasonal, interannual and decadal drivers of tree and grass productivity in an Australian tropical savanna. Global Change Biology 24, 2530-2544.

Moss, P.T. (2013) Treatise on Geomorphology, in: AD Shroder, D.K.A.S. (Ed.), Palynology and its application to geomorphology. Academic Press, San Diego, San Diego, California, U.S.A., pp. 315 - 335

Moss, P.T., Dunbar, G.B., Thomas, Z., Turney, C., Kershaw, A.P. and Jacobsen, G.E. (2017) A 60 000-year record of environmental change for the Wet Tropics of north-eastern Australia based on the ODP 820 marine core. Journal of Quaternary Science 32, 704-716

Moss, P.T. and Kershaw, A.P. (2000) The last glacial cycle from the humid tropics of northeastern Australia: comparison of a terrestrial and a marine record. Palaeogeography Palaeoclimatology Palaeoecology 155, 155-176.

Moss, P.T. and Kershaw, P.A. (2007) A late Quaternary marin palynological record (oxgyen isotope stages 1 to 7) for the humid tropics of northeastern Australia based on ODP site 820. Palaeogeography Palaeoclimatology Palaeoecology 251, 4-22.

Muller, J., McManus, J.F., Oppo, D.W. and Francois, R. (2012) Strengthening of the Northeast Monsoon over the Flores Sea, Indonesia, at the time of Heinrich event 1. Geology 40, 635-638.

Nanson, G.C., Price, D.M., Short, A.A., Young, R.W. and Jones, B.G. (1991) Comparative uranium-thorium dating and thermoluminescence dating of weathered Quaternary alluvium in the tropics of northern Australia. Quaternary Research 35, 347-366.

Nesbitt, H.W., Markovics, G. and price, R.C. (1980) Chemical processes affecting alkalis and alkaline earths during continental weathering. Geochimica et Cosmochimica Acta 44, 1659-1666.

Nicholls, N. (1995) All-India Summer Monsoon Rainfall and Sea Surface Temperatures around Northern Australia and Indonesia. Journal of Climate 8, 1463-1467.

Nicholls, N., McBride, J.L. and Ormerod, R.J. (1982) On Predicting the Onset of the Australian Wet Season at Darwin. Monthly Weather Review 110, 14-17.

Nott, J. and Price, D.M. (1994) Plunge pools and palaeoprecipitation. Geology 22, 1047-1050.

O'Leary, M. (1988) Carbon isotopes in photosynthesis Bioscience 38, 328 - 336.

Olsen, J., Anderson, N.J. and Leng, M.J. (2013) Limnological controls on stable isotope records of late-Holocene palaeoenvironment change in SW Greenland: a paired lake study. Quaternary Science Reviews 66, 85-95.

Partin, J.W., Cobb, K.M., Adkins, J.F., Clark, B. and Fernandez, D.P. (2007) Millennial-scale trends in west Pacific warm pool hydrology since the Last Glacial Maximum. Nature 449, 452-455.

Petheram, C., McMahon, T.A. and Peel, M.C. (2008) Flow characteristics of rivers in northern Australia: Implications for development. Journal of Hydrology 357, 93-111.

Pietsch, B. (1989) 1:100 000 Geological Map Series Explanatory Notes Reynolds River 5071, , Darwin. Government Printer of the Northern Territory, Darwin.

Pietsch, B.A. and Edgoose, C.J. (1988) The stratigraphy, metamorphism and tectonics of the Early Proterozoic Litchfield Province and western Pine Creek Geosyncline, Northern Territory. Precambrian Research 40-41, 565-588.

Pitman, A.J. and Hesse, P.P. (2007) The significance of large-scale land cover change on the Australian palaeomonsoon. Quaternary Science Reviews 26, 189-200.

Pope, M., Jakob, C. and Reeder, M.J. (2009) Regimes of the North Australian Wet Season. Journal of Climate 22, 6699-6715.

Preece, N.D. (2013) Tangible evidence of historic Australian indigenous savanna management. Austral Ecology 38, 241-250.

Prior, L.D., Eamus, D. and Bowman, D.M.J.S. (2004) Tree growth rates in north Australian savanna habitats: seasonal patterns and correlations with leaf attributes. Australian Journal of Botany 52, 303-314.

Prior, L.D., Murphy, B.P. and Russell-Smith, J. (2009) Environmental and demographic correlates of tree recruitment and mortality in north Australian savannas. Forest Ecology and Management 257, 66-74.

Reeves, J.M., Chivas, A.R., García, A., Holt, S., Couapel, M.J.J., Jones, B.G., Cendón, D.I. and Fink, D. (2008) The sedimentary record of palaeoenvironments and sea-level change in the Gulf of Carpentaria, Australia, through the last glacial cycle. Quaternary International 183, 3-22.

Rice, D.L. and Tenore, K.R. (1981) Dynamics of carbon and nitrogen during the decomposition of detritus derived from estuarine macrophytes. Estuarine, Coastal and Shelf Science 13, 681-690.

Rossignol-Strick, M. (1985) Mediterranean Quaternary sapropels, an immediate response of the African monsoon to variation of insolation. Palaeogeography, Palaeoclimatology, Palaeoecology 49, 237-263.

Rowe, C., Brand, M., Hutley, L.B., Wurster, C., Zwart, C., Levchenko, V. and Bird, M. (2019) Holocene savanna dynamics in the seasonal tropics of northern Australia. Review of Palaeobotany and Palynology 267, 17-31.

Rowe, C., Wurster, C.M., Zwart, C., Brand, M., Hutley, L.B., Levchenko, V. and Bird, M.I. (2020) Vegetation over the last glacial maximum at Girraween Lagoon, monsoonal northern Australia. Quaternary Research, 1-14.

Ruddiman, W.F. (2006) What is the timing of orbital-scale monsoon changes? Quaternary Science Reviews 25, 657-658.

Sankaran, M., Hanan, N.P., Scholes, R.J., Ratnam, J., Augustine, D.J., Cade, B.S., Gignoux, J., Higgins, S.I., Le Roux, X., Ludwig, F., Ardo, J., Banyikwa, F., Bronn, A., Bucini, G., Caylor, K.K., Coughenour, M.B., Diouf, A., Ekaya, W., Feral, C.J., February, E.C., Frost, P.G.H., Hiernaux, P., Hrabar, H., Metzger, K.L., Prins, H.H.T., Ringrose, S., Sea, W., Tews, J., Worden, J. and Zambatis, N. (2005) Determinants of woody cover in African savannas. Nature 438, 846-849.

Shiau, L.-J., Chen, M.-T., Clemens, S.C., Huh, C.-A., Yamamoto, M. and Yokoyama, Y. (2011) Warm pool hydrological and terrestrial variability near southern Papua New Guinea over the past 50k. Geophysical Research Letters 38.

Shulmeister, J. and Lees, B.G. (1995) Pollen evidence from tropical Australia for the onset of an ENSO-dominated climate at c. 4000 B.P. The Holocene 5, 10-18.

Staver, A.C., Archibald, S. and Levin, S.A. (2011a) The global extent and determinants of savanna and forest as alternative biome states. Science 334, 230-232.

Staver, A.C., Bond, W.J. and February, E.C. (2011b) History matters: tree establishment variability and species turnover in an African savanna. Ecosphere 2, art49.

Steinke, S., Mohtadi, M., Prange, M., Varma, V., Pittauerova, D. and Fischer, H.W. (2014) Mid- to Late-Holocene Australian–Indonesian summer monsoon variability. Quaternary Science Reviews 93, 142-154.

Stevenson, J., Brockwell, S., Rowe, C., Proske, U. and Shiner, J. (2015) The palaeo-environmental history of Big Willum Swamp, Weipa: An environmental context for the archaeological record. Australian Archaeology 80, 17-31.

Stewart, G., Turnbull, M., Schmidt, S. and Erskine, P. (1995) ^{13}C Natural Abundance in Plant Communities Along a Rainfall Gradient: a Biological Integrator of Water Availability. Functional Plant Biology 22, 51-55.

Stott, L., Cannariato, K., Thunell, R., Haug, G.H., Koutavas, A. and Lund, S. (2004) Decline of surface temperature and salinity in the western tropical Pacific Ocean in the Holocene epoch. Nature 431, 56-59.

Trenberth, K.E., Stepaniak, D.P. and Caron, J.M. (2000) The Global Monsoon as Seen through the Divergent Atmospheric Circulation. Journal of Climate 13, 3969-3993.

van der Kaars, S., De Deckker, P. and Gingele, F.X. (2006) A 100 000-year record of annual and seasonal rainfall and temperature for northwestern Australia based on a pollen record obtained offshore. Journal of Quaternary Science 21, 879-889.

van der Kaars, W.A. (1991) Palynology of eastern Indonesian marine piston-cores; a late Quaternary vegetational and climatic record for Australasia. Palaeogeography, Palaeoclimatology, Palaeoecology 85, 239-302.

Vidic, N.J. and Montanez, I.P. (2004) Climatically driven glacial-interglacial variations in C-3 and C-4 plant proportions on the Chinese Loess Plateau, pp. 337-340.

Wang, G., Feng, X., Han, J., Zhou, L., Tan, W. and Su, F. (2008a) Paleovegetation reconstruction using δ13C of Soil Organic Matter. Biogeosciences Discussions 5, 1795-1823.

Wang, Y., Cheng, H., Edwards, R.L., Kong, X., Shao, X., Chen, S., Wu, J., Jiang, X., Wang, X. and An, Z. (2008b) Millennial- and orbital-scale changes in the East Asian monsoon over the past 224,000 years. Nature 451, 1090-1093.

Wang, Y.J., Cheng, H., Edwards, R.L., An, Z.S., Wu, J.Y., Shen, C.-C. and Dorale, J.A. (2001) A High-Resolution Absolute-Dated Late Pleistocene Monsoon Record from Hulu Cave, China. Science 294, 2345-2348.

Warfe, D.M., E., P.N., Davies, P.M., J., P.B., Hamilton, S.K., Kennard, M.J., Townsend, S.A., P., B., Ward, D.P., Douglass, M.M., Burford, M.A., M., F., Bunn, S.E. and Halliday, I.A. (2011) The 'wet–dry' in the wet–dry tropics drives river ecosystem structure and processes in northern Australia. Freshwater Biology 56, 2169-2195.

Weldeab, S., Lea, D.W., Schneider, R.R. and Andersen, N. (2007) 155,000 Years of West African Monsoon and ocean thermal evolution. Science 316, 1303-1307.

Weltje, G.J. and Tjallingii, R. (2008) Calibration of XRF core scanners for quantitative geochemical logging of sediment cores: Theory and application. Earth and Planetary Science Letters 274, 423-438.

Wende, R., Nanson, G.C. and Price, D.M. (1997) Aeolian and fluvial evidence for late Quaternary environmental change in the east Kimberley of western Australia. Australian Journal of Earth Sciences 44, 519-526.

White, D.S. and Howes, B.L. (1994) Nitrogen incorporation into decomposing litter of Spartina alterniflora. Limnology and Oceanography 39, 133-140.

Williams, A.N., Ulm, S., Goodwin, I.D. and Smith, M. (2010) Hunter-gatherer response to late Holocene climatic variability in northern and central Australia. Journal of Quaternary Science 25, 831-838.

Williams, A.N., Veth, P., Steffen, W., Ulm, S., Turney, C.S.M., Reeves, J.M., Phipps, S.J. and Smith, M. (2015) A continental narrative: Human settlement patterns and Australian climate change over the last 35,000 years. Quaternary Science Reviews 123, 91-112.

Williams, R.J., Duff, G.A., Bowman, D.M.J.S. and Cook, G.D. (1996) Variation in the composition and structure of tropical savannas as a function of rainfall and soil texture along a large-scale climatic gradient in the Northern Territory, Australia. Journal of Biogeography 23, 747-756.

Wu, J., Wang, Y., Cheng, H. and Edwards, L.R. (2009) An exceptionally strengthened East Asian summer monsoon event between 19.9 and 17.1 ka BP recorded in a Hulu stalagmite. Science in China Series D: Earth Sciences 52, 360-368.

Wynn, J.G. and Bird, M.I. (2007) C4-derived soil organic carbon decomposes faster than its C3 counterpart in mixed C3/C4 soils. Global Change Biology 13, 2206-2217.

Wyrwoll, K.-H. and Valdes, P. (2003) Insolation forcing of the Australian monsoon as controls of Pleistocene mega-lake events. Geophysical Research Letters 30.

Wyrwoll, K.H. and Miller, G.H. (2001) Initiation of the Australian summer monsoon 14,000 years ago. Quaternary International 83-85, 119-128.

Yan, H., Wei, W., Soon, W., An, Z., Zhou, W., Liu, Z., Wang, Y. and Carter, R.M. (2015) Dynamics of the intertropical convergence zone over the western Pacific during the Little Ice Age. Nature Geoscience 8, 315-320.

Yan, M., Wang, B., Liu, J., Zhu, A., Ning, L. and Cao, J. (2018) Understanding the Australian Monsoon change during the Last Glacial Maximum with a multi-model ensemble. Clim. Past 14, 2037-2052.

Yokoyama, Y., Purcell, A., Lambeck, K. and Johnston, P. (2001) Shore-line reconstruction around Australia during the Last Glacial Maximum and Late Glacial Stage. Quaternary International 83-85, 9-18.

Yuan, D., Cheng, H., Edwards, R.L., Dykoski, C.A., Kelly, M.J., Zhang, M., Qing, J., Lin, Y., Wang, Y., Wu, J., Dorale, J.A., An, Z. and Cai, Y. (2004) Timing, Duration, and Transitions of the Last Interglacial Asian Monsoon. Science 304, 575-578.

Figure captions

Figure 1. Location and environment of Table Top Swamp (TTS). **a)** Position of Table Top Swamp in the 'Top End' of the Northern Territory. The approximate position of the ITCZ during the Austral summer is shown on the map. The numbered dots on the panel show the location of other studies the data from which is plotted in figures 6-8, where 1 is the Ball Gown and KN1-51 speleothems from the Kimberley, (Denniston et al., 2017), 2 is Black Springs (Field et al., 2017; Field et al., 2018; McGowan et al., 2012) and 3 and 4 are marine cores MD01-2778 and SO185-18479, respectively (Kuhnt et al., 2015). **b)** Satellite image of Table Top swamp (Google Earth), the position from where the core was collected is marked by a cross. The mesic vegetation surrounding the swamp is visible due its brighter green colour and greater tree density in comparison to the browner and more grass dominated savanna. **c)** Image of the swamp at the end of the wet season when it contains water and a dense cover of aquatic reeds (*Typha* sp). **d)** Image of the swamp at the end of the dry season. Note the polygonal cracks appearing on the swamp floor. **e)** Vegetation at the mesic forest/savanna interface.

Figure 2: Sedimentary and geochemical characteristics of TTS. **a)** Core photo with the main stratigraphic units indicated (see text for details). **b)** Grain size composition expressed as the percentage of sand silt and clay. **c)** Organic elemental composition, including Total Organic Carbon (TOC), C/N ratios, $\delta^{13}C_{TOC}$ (VPDB) and $\delta^{15}N$ (AIR). **d)** μXRF counts of selected elements presented as central normalised log ratios. Counts are plotted smoothed with a ten point running mean (solid lines) with the non-smoothed data are plotted behind in grey. Note 0 counts were removed from the Sr data for plot clarity.

Figure 3. Pollen abundance in the TTS core. The core image and main stratigraphic units are shown on the left of the diagram. Only taxa represented by a relative pollen abundance >2% are plotted. The full pollen assemblage is provided in Table S2.

Figure 4. Bayesian age/depth model for the TTS core derived using BACON model. OSL ages, ^{14}C AMS ages and dose rate normalised Ln/Tn ratios ($Ln/Tn\ DR_{norm}$) are also plotted. Four key chronological zones are represented on the plot by the vertical grey lines. These are: 1. Late MIS3 to Early MIS2; 2., The Last Glacial Maximum (LGM) through to Pleistocene/Holocene transition; 3., The Pleistocene/Holocene transition to Mid-Holocene; and 4., The Mid-Holocene to present. The sedimentary unit boundaries are indicated by the grey horizontal lines.

Figure 5. Modelled swamp moisture content at **a)** 18 ka, **b)** 12 ka and **c)** the present day. Data are expressed as a percentage of time, where full conditions equates the percentage of time where water volume is >90 of swamp capacity and dry conditions equates to the percentage of time where water volume is <10 % of swamp capacity.

Figure 6. Grainsize and element ratios plotted through TTS. Key physical parameters and selected previous records of ASM activity are plotted in panel a). The direction of likely increased ASM activity is indicated on each panel by blue arrows. The light green bar indicates the region of greatest age uncertainty. **a)** January insolation at 15 °S (Berger and Loutre, 1991), sea level (relative to present day) in Joseph Bonaparte Gulf (Yokoyama et al., 2001) and sea surface temperature (SST) reconstructed from Mg/Ca in marine core MD98-2170 from the Timor Sea and MD98-2176 from the Arafura Sea (Stott et al., 2004). Panels b)

to d) display data from TTS, including; **b)** Grainsize, **c)** Si/Ti and Sr/Ca ratios and, **d)** Y/Ti and Ca/Ti ratios.

Figure 7. Carbon, nitrogen and associated parameters plotted against time through TTS. Key physical parameters and selected previous records of ASM activity are also plotted. The direction of likely increased ASM activity is indicated on each panel by blue arrows. The light green bar indicates the region of greatest age uncertainty. For panel **a)** see the Fig. 6 caption. **b)** Terrestrial runoff (In(k/Ca)) records from marine cores MD01-2778 and SO185-18479 (Timor Sea, see Fig. 1 for location) (Kuhnt et al., 2015). **c)** $\delta^{18}O$ from speleothems in the Ball Gown and KNI-51 caves (Kimberly, see Fig. 1 for location) (Denniston et al., 2017). **d)** Total Organic Carbon (TOC) and C/N ratios in TTS. **e)** $\delta^{15}N$ (AIR) values and $\delta^{15}N$ estimated rainfall at TTS. Rainfall was derived from $\delta^{15}N$ using the modern $\delta^{15}N$ rainfall relationship for Northern Australia from Bird et al., (2019). The uncertainty envelope (light blue) represents the Root Mean Square Error of Prediction (RMSEP). **f)** $\delta^{13}C$ (VPDB) values and the $\delta^{13}C$ predicted ratio of arboreal taxa (woody vegetation) to Poaceae (grass) (A/G) in TTS. The A/G (arboreal/grass taxa) ratio indicates the degree of 'woodiness' of the vegetation mosaic and was estimated using the modern relationship between $\delta^{13}C$ and A/P from Bird et al., (2019). The uncertainty envelope (light green) represents the RMSEP. **g)** The modelled percentage of C_3 vegetation through TTS (from Eq. 2 and 3). Fully corrected data incorporate changes to $\delta^{13}C$ values from decomposition, changing $[\delta^{13}C]_{atm}$, changing $[CO_2]_{atm}$ and the effect of rainfall on $\delta^{13}C$. Non-rainfall corrected data include the same corrections, except these were not corrected for rainfall. Non-corrected data contains no corrections. The window of uncertainty (pink) around the Fully corrected C_3 values represents the effect of ±20 % rainfall.

Figure 8. Selected variables plotted through TTS during the Holocene. Key physical parameters and selected previous records of ASM activity are also plotted on the figure. For panel **a)** description see Fig. 6 caption. **b)** Aeolian and fluvial flux into Black Springs, central Kimberly (McGowan et al., 2012). Panels **c)** to **g)** show data from TTS including; **c)** Sand content, Y/Ti ratios and modelled (Fully corrected) percentage of C_3 vegetation. **d)** Relative pollen abundance for selected taxa. **e)** The percentage of pyrophobic trees and pollen concentration. **f)** pyrophyllic grass and log charcoal counts. **g)** Pollen abundance by vegetation type.

Table 1. Vegetation $\delta^{13}C$ data from the Table Top Swamp catchment

Family/type	Genus/species	Component	$\delta^{13}C$	C/N
Proteaceae	*Grevillea pteridifolia*	Leaf	-32.01	50.0
Myrtaceae	*Melaleuca viridiflora*	Leaf	-32.90	68.5
Myrtaceae	*Eucalyptus tetradonta*	Leaf	-30.87	44.0
Proteacae	*Banksia dentata*	Leaf	-30.88	63.8
Cyperaceae	?	Leaf	-12.58	132.9
Myrtaceae	*Melaleuca viridiflora*	Bark	-29.05	54.6
Myrtaceae	*Eucalyptus tetradonta*	Bark	-29.05	60.0
Myrtaceae	*Eucalyptus tetradonta*	Bark	-27.23	19.3
Myrtaceae	*Melaleuca viridiflora*	Wood	-31.46	78.8
Cyperaceae	?	Reed	-28.56	83.1
Poaceae	?		-29.84	35.9
Floating peat			-30.12	26.8
Mixed		Leaf litter	-29.09	55.3
Mixed		Leaf litter	-31.35	54.5

Author statement.
William Reynolds: Conceptualization, Methodology, Formal analysis, Investigation, Data Curation, Writing - Original Draft, Writing - Review & Editing. **Samuel, K., Marx:** Conceptualization, Methodology, Formal analysis, Investigation, Data Curation, Writing - Original Draft, Resources, Visualization, Supervision, Project administration, Funding acquisition. **Jan-Hendrik May:** Conceptualization, Methodology, Formal analysis, Investigation, Data Curation, Writing - Review & Editing, Resources, Visualization, Supervision, Project administration, Funding acquisition. **Matthew S., Forbes:** Methodology, Formal analysis, Investigation, Writing - Original Draft, Writing - Review & Editing, Visualization. **Nicola Stromsoe:** Methodology, Formal analysis, Investigation, Writing - Original Draft, Writing - Review & Editing, Resources. **Michael-Shawn Fletcher:** Methodology, Formal analysis, Investigation, Writing - Review & Editing, Visualization. **Tim Cohen:** Writing - Review & Editing, Investigation, Resources, Supervision. **Patrick Moss:** Formal analysis, Investigation, Writing - Review & Editing, Resources. **Debashish Mazumder**: Formal analysis, Investigation, Writing - Review & Editing, Resources. **Patricia Gadd:** Formal analysis, Investigation, Writing - Review & Editing, Resources.

- Wetlands were likely very limited across the Top End and northern Australia before 25 ka with savanna significantly more grass dominated.
- The IASM became significantly more effective from 9ka, with ecosystem developing their current composition and configuration after this time.
- There is evidence of human resource use impacting vegetation assemblages in the Top End from the early to mid-Holocene.
- There is evidence of both increasing moisture and aridity in the mid- to late-Holocene in the Top End.
- Sea level appears to be the major control of IASM strength in the Top End over the past 35 ka.